LQR Control of Dual-Active Bridge DC-DC Power Electronic Converters

by

Christian Richard

Bachelors of Science in Electrical Engineering, UNB, 2017

A THESIS SUBMITTED IN PARTIAL FULFILLMENT OF THE REQUIREMENTS FOR THE DEGREE OF

Master of Science in Engineering

In the Graduate Academic Unit of Electrical Engineering

Supervisor:	Saleh Saleh, PhD, Electrical Eng.
Examining Board:	Julian Meng, Ph.D. Electrical Eng., Chair Bo Cao, Ph.D. Electrical Eng. Suprio Ray, Ph.D., Computer Science

This thesis is accepted

Dean of Graduate Studies

THE UNIVERSITY OF NEW BRUNSWICK

June, 2020

©Christian Richard, 2020

Abstract

Recent trends in power system operation have been constructed to implement controlled and bi-directional power flows on the load side. Such power flows have facilitated the implementation of the *load-follows-generation* new strategy for operating power systems. In addition, the successful implementation of controlled and bi-directional power flows has supported the integration of different types of distributed generation and storage (DGS) units. These new generation assets are typically interconnected to distribution systems by stages of power electronic converters (PECs). The back-to-back, modular, and solid-state transformers are examples of PEC topologies used to interconnect DGS units.

The major functions of PECs in DGS units, include converting, processing, and controlling the electric power to meet certain conditions imposed by the host grid. These conditions mandate the design of controllers to accurately and effectively operate stages of PECs in stable and reliable manners. Among the key PECs to implement controlled and bi-directional power flows are the conventional and resonant *dual active bridge (DAB)* dc PECs. These bi-directional dc PECs are widely used to construct active DC-links in many applications, such as voltage and reactive power compensation, motor drives, plasma generation units, etc. The employment of DAB dc PECs in power systems requires the design and implementation of accurate, fast, and reliable controllers.

This thesis aims to design, implement, and test linear-quadratic regulator (LQR)

controllers for the DAB and resonant DAB dc PECs. The design of an LQR controller is achieved by the development of linearized models for the DAB and resonant DAB dc PECs. These models are developed to accommodate the switching scheme, as well as the relationship between the duty cycle and reference voltages. Furthermore, the developed models for DAB and resonant DAB dc PECs are used to devise a tuning procedure for the designed LQR controllers.

The performance of the designed LQR controllers is tested for the DAB and the resonant DAB dc PECs under different conditions. Tested conditions include step changes in the power flow, changes in the voltage on the input side of the PEC, and bi-directional power flows. The results of these tests show that designed LQR controllers can operate DAB and resonant DAB dc PECs to adjust input and output voltages during step changes in the power flow, changes in the direction of the power flow, and changes in the voltage. Observed performance features are also compared with other controllers under similar conditions. Test and comparison results demonstrate the efficacy of the designed LQR controllers to operate DAB and resonant DAB dc PECs under different loading and dynamic conditions.

Acknowledgments

I am extremely grateful to my supervisor Dr. Saleh Saleh for his support and guidance throughout my studies and this thesis. Dr. Saleh has encouraged me to get out of my comfort zone, to reach my fullest potential, and he always had confidence in my work.

I would like to thank my parents for their support during my studies.

I also wish to express my gratitude for scholarship and funding opportunities given to me by NSERC-NEST, Emera Inc., New Brunswick Innovation Foundation (NBIF), and the University of New Brunswick.

Contents

Abstract ii

Acknowledgements iv

Contents v

List of Tables viii

List of Figures ix

1 Introduction 1

1.1 General 1

1.2 Motivation 2

1.3 Literature Review 3

1.4 Thesis Objectives 8

1.5 Thesis Outline 8

2 Modeling the Dual Active Bridge Converter 10

2.1 General 10

2.2 DAB Converter 11

2.3 DAB Converter Model 14

2.4 Switching Scheme 17

2.4.1 Including the Switching Scheme in the State-Space Model of the DAB PEC 20

2.5 Summary 22

3 State Feedback Control for DAB PEC **23**

3.1 General 23

3.2 Linear Quadratic Regulator 24

3.2.1 LQR Model 24

3.2.2 Integral Action 26

3.3 LQR for DAB PEC 27

3.3.1 Tuning the LQR 27

3.3.2 The Structure of the Designed LQR 28

3.4 Summary 30

4 Performance of the LQR Based Controller **31**

4.1 General 31

4.2 Simulation Model 32

4.2.1 Determining Parameters of LQR Controllers 32

4.2.2 Constructed Models for the DAB and Resonant DAB 35

4.3 Simulated Performance 36

4.3.1 DAB Performance Tests 36

4.3.2 Resonant DAB Performance Tests 42

4.4 Summary 48

5 Summary and Conclusions **50**

5.1 Summary 50

5.2 Conclusions 51

5.3 Contributions 52

5.4 Future Work 52

Bibliography **54**

A Additional Test Cases **59**

A.1 DAB PEC with Different Ratings 59

A.2 Combined DAB PECs 63

Curriculum Vitae

List of Tables

4.1 Data for the Constructed SIMULINK models of the Conventional and Resonant DAB PECs 35

A.1 Parameters of the DAB PEC Model 60

List of Figures

1.1 Diagram of the three stages solid-state transformer and their connection to the power grid. 3

2.1 Circuit Diagram of DAB Converter 12

2.2 Example of Voltage and Current Waveform 13

2.3 Circuit Diagram of Resonant DAB Converter 14

2.4 Sample waveforms for V_P and V_S over one cycle of operating the DAB PEC. The notation d_p denotes the duty cycle of V_p, d_s denotes the duty cycle of V_S, and d_θ denotes to the phase shift between V_p and V_s. 18

2.5 The simulated open-loop operation of the DAB PEC: the primary side and secondary sides voltages. 19

2.6 The simulated open-loop operation of the DAB PEC: the currents flowing on the medium and low voltage sides of the HFT, along with the current flowing through the HFT itself. 19

3.1 Control system block diagram of the DAB PEC system with its LQR 29

3.2 Block Diagram of the DAB PEC controller with sensor inputs and switching scheme command outputs 30

4.1 The steady-state responses of the conventional DAB PEC with the designed LQR controller. The per-unit currents I_1 and I_2 (base current is 0.69 A), per-unit reference and actual voltage on the low voltage side of the HFT (base voltage is 360 V), and per-unit voltage commands ΔV_1 and ΔV_2 (base voltage is 360 V). 37

4.2 Responses of the conventional DAB PEC with the designed LQR controller to step changes in load power demands. The per-unit currents I_1 and I_2 (base current is 0.69 A), per-unit reference and actual voltage on the low voltage side of the HFT (base voltage is 360 V), and per-unit voltage commands ΔV_1 and ΔV_2 (base voltage is 360 V). . . 38

4.3 Responses of the conventional DAB PEC with a PI controller to step changes in load power demands. The per-unit currents I_1 and I_2 (base current is 0.69 A), per-unit command and actual voltage on the low voltage side of the HFT (base voltage is 360 V), and per-unit voltage commands ΔV_1 and ΔV_2 (base voltage is 360 V). 40

4.4 Responses of the conventional DAB PEC with the designed LQR controller to step changes in the supply voltage while supporting a 200 W load. The per-unit currents I_1 and I_2 (base current is 0.69 A), per-unit reference and actual voltage on the low voltage side of the HFT (base voltage is 360 V), and per-unit voltage commands ΔV_1 and ΔV_2 (base voltage is 360 V). 41

4.5 The steady-state responses of the resonant DAB PEC with the designed LQR controller. The per-unit currents I_1 and I_2 (base current is 0.69 A), per-unit reference and actual voltage on the low voltage side of the HFT (base voltage is 360 V), and per-unit voltage commands ΔV_1 and ΔV_2 (base voltage is 360 V). 43

4.6 Responses of the resonant DAB PEC with the designed LQR controller to step changes in load power demands. The per-unit currents I_1 and I_2 (base current is 0.69 A), per-unit reference and actual voltage on the low voltage side of the HFT (base voltage is 360 V), and per-unit voltage commands ΔV_1 and ΔV_2 (base voltage is 360 V). . . 45

4.7 Responses of the resonant DAB PEC with the designed LQR controller to step changes in the supply voltage while supporting a 200 W load. The per-unit currents I_1 and I_2 (base current is 0.69 A), per-unit reference and actual voltage on the low voltage side of the HFT (base voltage is 360 V), and per-unit voltage commands ΔV_1 and ΔV_2 (base voltage is 360 V). 47

A.1 Responses of the conventional DAB PEC with the designed LQR controller to step changes in load power demands. The per-unit currents I_1 and I_2 (base current is 5 A), per-unit reference and actual voltage on the low voltage side of the HFT (base voltage is 660 V), and per-unit voltage commands ΔV_1 and ΔV_2 (base voltage is 660 V). . . 61

A.2 Responses of the conventional DAB PEC with the designed LQR controller to step changes in the supply voltage while supporting a 2640 W load. The per-unit currents I_1 and I_2 (base current is 5 A), per-unit reference and actual voltage on the low voltage side of the HFT (base voltage is 660 V), and per-unit voltage commands ΔV_1 and ΔV_2 (base voltage is 660 V). 63

A.3 Responses of three combined conventional DAB PECs with the designed LQR controller to step changes in load power demands. The per-unit reference and actual voltage on the low voltage side of the HFT (base voltage is 360 V). 65

A.4 Responses of three conventional DAB PECs with the designed LQR controller to step changes in the supply voltage while supporting a 600 W load. The per-unit reference and actual voltage on the low voltage side of the HFT (base voltage is 360 V) 65

Chapter 1

Introduction

1.1 General

The main function of a distribution power transformer is to connect low and medium voltage loads with a power system distribution network. This function of distribution power transformer has been implemented by different designs of magnetic core-type, two-windings, low-frequency power transformers. These power transformers have been widely used due to their simple design and maintenance, reliability, efficiency, availability in different ratings and configurations, and easy grounding [1–5]. Despite these structural and operational advantages, core-type distribution power transformers are not capable of offering grid support functions or ancillary services, such as voltage and frequency support, power factor correction, demand response, improving power quality, and/or providing dc distribution terminals [1–6].

As of late, several power systems have been shifting their operation toward increased levels of the de-regulated operation, where load demands can be controlled and different types of distributed generation can be integrated [5, 6]. In addition, some power systems have shown growing interests in integrating dc micro-grids, and providing a dc distribution as part of their load-side power delivery [1–3]. Such new functions by distribution systems can not be accommodated by conventional core-type dis-

tribution power transformers. In addition, the growing interests in interconnection storage systems as parts of the active demand response mandate controlling the power flow through a distribution transformer [1–6]. The aforementioned new functions in the distribution system can be achieved by solid state transformers (SSTs), which are constructed using back-to-back power converters that are separated by a dc-link [6]. These new breeds of distribution transformers can be designed with different topologies [5, 6]. Nonetheless, the existence of a dc-link in a SST can offer different advantages, including the control of the power flow, providing dc distribution, integrating storage systems, and improving power quality [1–6].

1.2 Motivation

The motivation for this research arises from needs to operate distribution transformers with control actions to achieve various grid support functions. In addition, desired control actions can be set to offer bi-directional power flow, thus implementing an active demand response. Such control actions can be designed and implemented at the ac-dc converter, dc-link, and/or dc-ac converter. This research work intends to focus on designing, implementing, and testing controllers for the dc-link stage of solid-state distribution transformers to achieve grid support functions and active demand responses.

1.3 Literature Review

The generic structure for a SST, visualized in Figure 1.1, is composed from three stages; the medium voltage (MV) side, the dc-link, and low voltage (LV) side. The design, control, and operation of each stage can implemented to achieve different functionalities, which may include a uni-directional or a bi-directional power flow, a passive or an active dc-link, support for dc distribution, isolated MV and LV sides, and a single-phase or a three phase LV side [1–4]. The three-stage structure of SSTs can offer numerous advantages over core-type power transformers. Among such advantages is the use of the dc-link as a mid-stage between the MV and LV sides. The dc-link (passive or active) can facilitate an independent control of the power electronic converters (PECs) deployed on the MV and LV sides [5–8]. In addition, the dc-link, when designed as an active one, can facilitate implementing control actions, which are usually set to offer voltage and frequency support, isolating the MV and LV sides, and ancillary services for the LV and/or MV sides [4–7]. Furthermore, control actions in the dc-link stage, can be set to accommodate integrating distribution generation units (such small solar power units and/or energy storage units). This research work will focus on designing and testing controllers of active dc-links in SSTs that are employed in distribution systems.

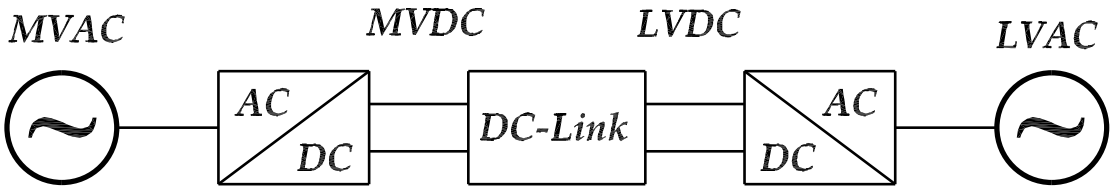

Figure 1.1: Diagram of the three stages solid-state transformer and their connection to the power grid.

In general, dc-links have a similar pattern of operation where switching elements

control the flow of energy into a reactive energy storage stage and out to an output filter. For the output filter, a capacitor or a capacitor bank are the most commonly used because it is simple and inexpensive. The sources of variation for these dc-links are how the flow of energy is controlled and the configuration of the reactive energy storage stage. Because of the reactive energy storage stage and the output filter, dc-links are at minimum a second order system. For example, the buck converter and the boost converter use a single switch to regulate the flow of energy and an inductor for the reactive energy storage stage. [24]

For SSTs, there are requirements and performance goals that limit the possible options for dc-links. The requirements for a dc-link are galvanic isolation, bidirectional power flow, high power ratings and low cost. The main performance goal for this application is efficiency and the ability to handle input and output variations. One of the few dc-link structure that can meet those requirements is the Dual Active Bridge (DAB) converter that works by passing energy through a high frequency transformer (HFT) [9–11, 28, 29]. Since this dc-link uses multiple switches, there are a few different switching schemes with advantages and drawbacks that can be used. The three basic switching schemes for the DAB converter are single phase shift (SPS), the dual phase shift (DPS), and the triple phase shift (TPS) [10–12, 29]. The basic tradeoff with these schemes is that each additional phase shift provides more control over the operation of the dc-link, but that comes at the cost of additional control inputs that increases the complexity of the controller needed [11, 13]. For the context of this research work, a switching scheme such as DPS or TPS with multiple control inputs will be preferable because it can focus on voltage regulation and efficient operation at the simultaneously.

The design of a controller typically considers the operation, functional limits, and

desired outputs of the controlled system. For power systems applications, the design priorities for a controller of the dc link, in a SST, are to regulate the output dc voltage, maximize efficiency, and to protect against overloading and voltage fluctuations [14]. In general, the design of a controller for any system can be constrained by desired performance (steady-state, overshoot, rising time, settling time, etc.), implementation platform (digital circuits, digital signal processors, micro-controllers, etc.), cost, level of complexity, and level of adaptability. On one hand, simple controllers may not completely achieve desired performance, but they enjoy easy design and implementation. On the other hand, complex controllers can offer significant performance, however, they suffer difficult designs and implementation. Another class of controllers is defined as adaptable controllers, which are controllers designed and implemented to vary its control law based on the state of the controlled system. Other controllers are defined as predictive controllers, which are designed and implemented to predict the deviation in the system response from its command value.

The aforementioned controller classes can be deployed for operating an active dc link that implements the dc stage in a SST. The bang-bang (hysteresis) controller is a popular controller for a wide range of system applications. This controller has the advantages of simple design and reduced implementation requirements. Nonetheless, bang-bang controllers are not preferred for operating dc-dc PECs due to the resulting non-linear relationship between the control variable (inductor current) and required switching signals to ensure the desired output.

Proportional-integral-derivative (PID) controllers are categorized as simple linear controllers, which can be used to operate various types of systems under different conditions and requirements. The design of a PID controller is usually carried out considering a linearized model of the controlled system. The linear modeling of the

controlled system is required to select the parameters of any PID controller (the gain, integrator gain, and derivative gain). The PID controller parameters can be selected using well developed methods, including the ZieglerNichols [25], Tyreus-Luyben [26], Software tools, CohenCoon, and Astrom-Hagglund methods [27]. There are modern methods (e.g. fuzzy sets, signal processing based methods, frequency domain methods, etc.) that have been used to select the parameters of PID controllers. For most dc-dc PEC, the inputs to a PID controller are the output voltage and inductor current, while its output is a duty cycle to generate the required pulse-width-modulated (PWM) switching signals. For this type of application, a PID controller can be digitally implemented and integrated with digital PWM switching signal generators. However, most dc-dc PECs are considered nonlinear systems, where PID controllers can suffer limited performance as a result of operating them outside the linear range. In order to overcome such a challenge, PID controllers are designed with multi-loop structures to segment the desired control actions, thus controlling the system as if it was almost linear [15]. This approach has been widely used in dc-dc PECs, where one control loop responds to large deviations between the desired output and its command, while another control loop responds to small deviations. Other improvements to the PID controllers have been based on including additional components, including a resonant component, observers, disturbance estimators, etc. [16]. References [15] and [16] presents various examples of employing PID controllers to operate dc-dc PECs. Furthermore, reference [17] extends the application of PID controllers to active dc-dc PECs. In these works, PID controllers have demonstrated good abilities to initiate fast, accurate, and reliable responses to changes in command values and/or deviations in desired outputs. However, PID controllers operating dc-dc converters suffered limited accuracy under changes in system parameters [18, 19]. In addition, PID controllers are mostly designed for a single control objective that can

be suitable for operating single-input switching schemes. Nonetheless, such a design can become a major limitation for operating multi-input switching schemes that are used in several PECs, including DAB converters. State feedback controllers, such as the linear-quadratic-regulator (LQR), have shown promising capabilities to operate systems with multiple states and inputs, where certain states are prioritized over others. In the case of dc-dc converters, the output voltage and input current are usually prioritized over intermediary states. In order to provide additional flexibility to other parameters (such as the load current and the input voltage), the LQR can be expanded to function within a defined range of parameter values [20]. A minor issue with LQR is the iterative design process of the controller since the priorities used in the design are not numerically defined by a fixed set of rules or equations [21].

The previous review has discussed the existing controllers for operating active dc-links for industrial applications, including SSTs. The DAB has been identified as a candidate for implementing active and bi-directional dc-links in SSTs. In order to achieve the desired SST functionalities, an adequate controller is required to operate the DAB employed in SSTs. Such a controller has to overcome the limitations of PID and heuristic controllers, when deployed to operate systems with multiple inputs and outputs and multiple states. The LQR has shown good ability to operate systems with multiple states, while offering a simple design. This controller can be designed and tuned to adequately operate a DAB that is employed in a SST to ensure facilitating its desired functionalities.

1.4 Thesis Objectives

This research work aims to design, implement, and test a LQR for DAB converter that is employed to implement a bi-directional active dc-link in a SST. The constraints for designing the desired LQR are set to achieve simple implementation, accurate and dynamic responses, and a wide stability margin. In addition, the desired LQR is to be operated to reduce circulating current losses, while providing a regulated output voltage for bi-directional mode.

1.5 Thesis Outline

This thesis will present the following parts:

- Chapter 2 presents the modeling of the DAB converter along with its resonant variant and the modeling for their switching schemes. This will provide insight for what form a controller would need to take in order to interact with both the model and the switching scheme.
- Chapter 3 develops the LQR controller for the DAB converter. The central focus of the controller will be for its use in a SST where it needs to handle grid conditions and prioritize efficient operation.
- Chapter 4 presents a simulation based performance analysis of the developed controller. The performance evaluations focuses on the controller's ability to handle input voltage variations, react to load changes, and operate efficiently in steady-state conditions.

- Chapter 5 summarizes the thesis, and draws conclusions based on the performance of the LQR controller. This chapter also presents research contributions, along with suggestions for future research works.

Chapter 2

Modeling the Dual Active Bridge Converter

2.1 General

Several industrial systems have shown a growing interests in bi-directional and controlled dc links. Among such systems are the grid-connected battery storage systems and solid-state power transformers. The interests in bi-directional and controlled dc-links are founded on the simple and accurate regulation of voltages and currents, which can be translated into voltage and frequency support on the ac sides. Such desired dc-links have to offer high power ratings, large voltage ratios between both sides, galvanic isolation, and bidirectional operation. Conventional dc-dc power electronic converters (PECs) can suffer limited power ratings (due to the storage size and impacts), bounded voltage ratios (due to imperfect components), and absence of galvanic isolation between input and output sides. In order to overcome the limitations of conventional dc-dc PECs, a transformer is required to implement a galvanic isolation, and accommodate the deployment of multiple PECs for high power ratings. A dc-link that can feature a transformer with multiple PECs can be sought to meet the operational and control requirements for battery storage systems and

solid-state power transformers. One of possible candidates to design such dc links is the dual active bridge (DAB), which is an isolated and bi-directional PEC.

The DAB is a dc-dc PEC that is designed with a high frequency transformer (HFT). This PEC converts its input dc voltage into a high frequency ac that is applied on the primary side of the HFT, and converts the secondary side ac voltage of the HFT into dc as its output. The input and output sides of the DAB PEC are constructed using H-bridges, thus offering a simple PEC design. Despite its simple structure and operation, the modeling of the DAB PEC can be challenging, as this PEC has dc and ac currents and voltages. This chapter discusses the structure, operation, and modeling of the DAB PEC. Furthermore, this chapter identifies a model for the DAB PEC that can be used for designing control systems.

2.2 DAB Converter

The DAB bridge converter can conveniently be divided into different sections, each of which can be operated individually. Figure 2.1 shows the circuit diagram for the DAB PEC, where a symmetry on both sides of the HFT can be noticed. Both sides (the medium voltage and low voltage) of a DAB PEC are equipped with shunt capacitors that block harmonic currents from flowing into or out of the DAB converter. These harmonic currents are usually created by switching actions of the H-bridges. As the DAB PEC is operated at a high frequency, these two capacitors have small values compared to low frequency PECs. The two H-bridges on both sides of the HFT can be operated to convert dc into ac or ac into dc. Each H-bridge is composed of four controlled switching elements that can accommodate high switching frequencies. Insulated gate bipolar transistors (IGBTs), and Metal Oxide Semiconductor

Field-Effect Transistors (MOSFETs) are among the popular switching elements used to construct DAB PECs. The HFT is used to change step-up or step-down the voltage, as well as to provide a galvanic isolation between both H-bridges. The selection for a HFT, in a DAB PEC, is based on the switching frequency of the H-bridges and power ratings of the DAB PEC. A high switching frequency can reduce the size and cost of the HFT, while limiting the power ratings of the DAB PEC.

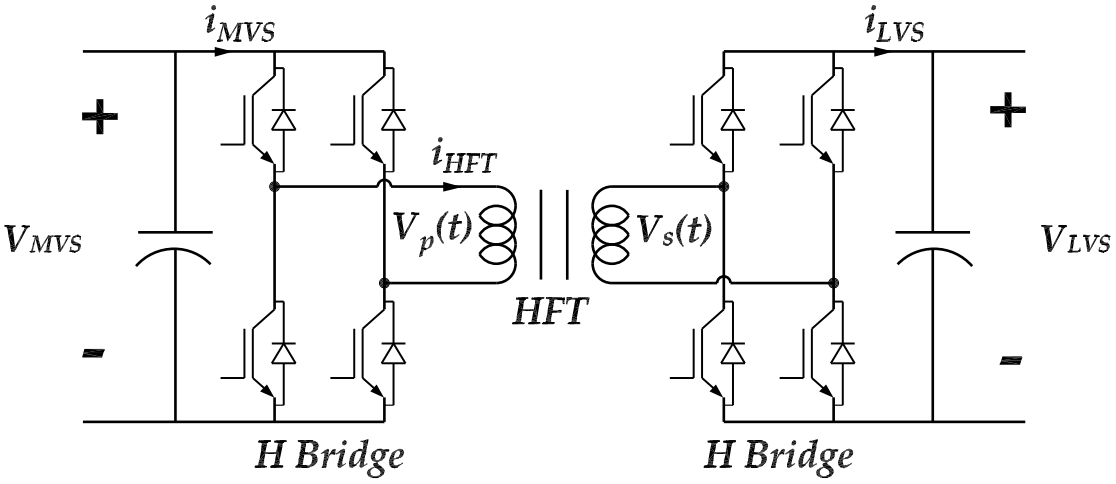

Figure 2.1: Circuit Diagram of DAB Converter

In general, the HFT requires ac voltages on its primary and secondary windings for the power to be transferred from one side to the other. This requirement implies that both H-bridges have to process dc voltages into ac ones. Such processing can be achieved by operating the H-bridges to produce three different voltage levels at the primary and secondary windings of the HFT. These three levels can be created by allowing the sequential periodic alternation between the positive and negative dc voltages, along with a blanking time in between (see Figure 2.2). These periodic three voltage levels construct an ac voltage, which will take a rectangular waveform. It should be noted that the produced ac voltage will have harmonic components. However, since this ac voltage is converted back into dc at the output of the DAB,

voltage harmonic are suppressed by the capacitors on both sides of the HFT. Finally, the magnitude, frequency, and phase of the square-wave ac voltage can be adjusted using the switching scheme and/or the controller of the DAB.

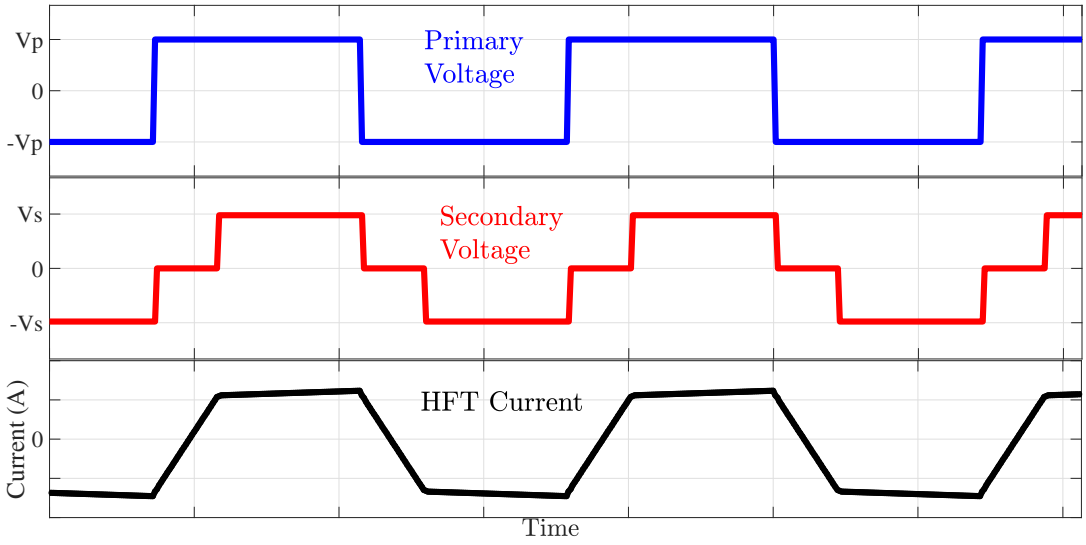

Figure 2.2: Example of Voltage and Current Waveform

The square-wave ac voltages created on both sides of the HFT will force a current to flow through the primary windings. This current will have a magnitude that depends on the power flowing through the HFT, while its frequency is dictated by the frequency of the square-wave ac voltage. Due to the high value of the equivalent inductance of a HFT, the rise and fall of the primary current will have a close-to linear nature. When the ac voltage undergoes the positive voltage level, the primary current will rise, and it will fall as the ac voltage undergoes the negative voltage level. During the blanking time (0 voltage level), the primary current will have a small decay due to the equivalent resistance of the HFT windings. Figure 2.2 shows an example for the primary current that will be produced by the primary and secondary ac voltages shown in the same figure.

A resonant capacitor can be added in series with the HFT, as show in Figure 2.3, to

create a resonant converter. The motivating reason for the resonant DAB PEC is to reduce switching losses [30, 31]. The resonant capacitor will change the impedance between the two H-Bridges. This will affect the amplitude and phase of the current. The shape of the HFT current waveform is a clean sinusoid. The practical limit for the addition of a resonance capacitor is the large required ratings for the capacitor since it needs to handle large ac currents.

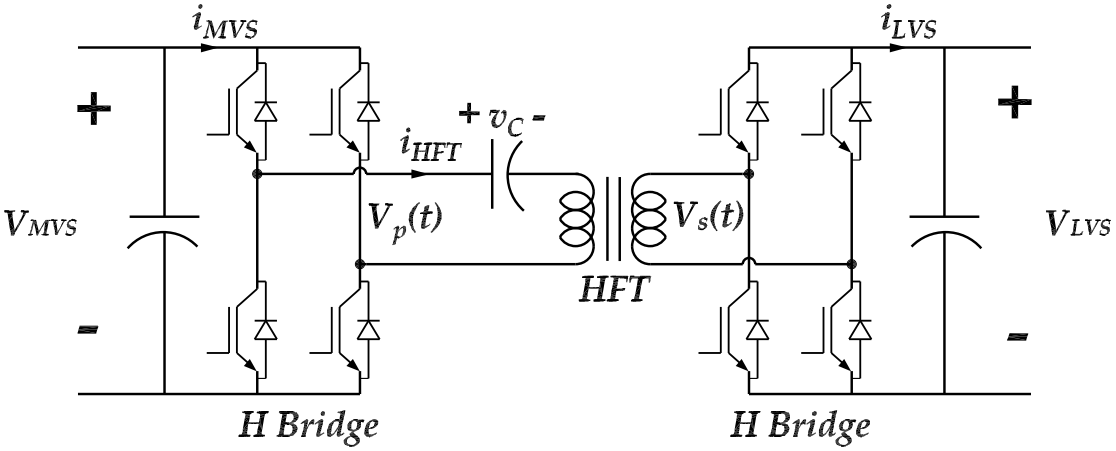

Figure 2.3: Circuit Diagram of Resonant DAB Converter

2.3 DAB Converter Model

The general approach to construct a model for a DAB PEC has been based on an averaged model over each cycle of the primary side ac voltage. This approach allows including both ac and dc quantities in the same space. In this modeling approach, ac voltages and currents are approximated as ideal ac waveforms, each of which has a magnitude and a phase. Magnitudes and phases of ac voltages and currents can be converted to phasors (real and imaginary components). This conversion leads to expressing each voltage and current (dc and ac) using a dc component, a real component, and an imaginary component. However, each voltage and current may

have one or two of its components with zero values. The averaged model approach can be translated into a state-space model as [22, 23]:

$$\begin{bmatrix} \dot{I}_1 \\ \dot{I}_2 \\ \dot{V}_{LVS} \end{bmatrix} = \begin{bmatrix} -\frac{R}{L} & \omega & 0 \\ -\omega & -\frac{R}{L} & 0 \\ \frac{2}{\pi C_{LVS}} & 0 & 0 \end{bmatrix} \begin{bmatrix} I_1 \\ I_2 \\ V_{LVS} \end{bmatrix} + \begin{bmatrix} \frac{1}{L} & 0 \\ 0 & \frac{1}{L} \\ 0 & 0 \end{bmatrix} \begin{bmatrix} \Delta V_1 \\ \Delta V_2 \end{bmatrix} \tag{2.1}$$

where R and L are the series resistance and inductance of the HFT, ω is the angular frequency of the square-wave ac voltage, and the states I_1 and I_2 represent the real and imaginary component of the HFT current. The voltage commands, ΔV_1 and ΔV_2, are the real and imaginary components of the voltage difference between V_p and V_s. They are called command voltages because the switching scheme is used to set V_p and V_s to values that matches ΔV_1 and ΔV_2 to the command voltages.

$$\Delta V_1 = (V_p)_{real} - (V_s)_{real} \tag{2.2}$$

$$\Delta V_2 = (V_p)_{imaginary} - (V_s)_{imaginary} \tag{2.3}$$

Remarks for equation 2.1:

- The equations for $\dot{I}_1$ and $\dot{I}_2$ are derived by applying a KVL loop around the primary side H bridge, the HFT, and the secondary side HFT. In this KVL the HFT is treated as a series RL circuit elements.
- The equation for $\dot{V}_{LVS}$ is derived is based on the current coming out of the secondary H bridge and charging the capacitor C_{LVS}.

Equation (2.1) is made with the following assumptions in order to obtain a linear

model:

i) The real and imaginary components represents components of an ideal ac waveforms.

ii) The real and imaginary components are relative to the secondary voltage.

iii) The secondary voltage is at its maximum amplitude which is the reason that the equation (2.1) for $\dot{V}_{LVS}$ is linear.

Assumptions i and ii are shown in the equations below where the subscript '1' represents the real component and the subscript '2' represents the imaginary component. The time in those equations is relative to the secondary voltage $V_s(t)$.

$$i_{HFT}(t) \approx I_1 cos(\omega t) + I_2 sin(\omega t) \tag{2.4}$$

$$v_C(t) \approx V_1 cos(\omega t) + V_2 sin(\omega t) \tag{2.5}$$

In the resonant DAB PEC, equation (2.1) has to be modified to accommodate the dynamics, which are created by the resonance capacitor. The state space equation for the resonant DAB PEC can be stated as [23]:

$$\begin{bmatrix} \dot{V}_1 \\ \dot{V}_2 \\ \dot{I}_1 \\ \dot{I}_2 \\ \dot{V}_{LVS} \end{bmatrix} = \begin{bmatrix} 0 & \omega & \frac{1}{C} & 0 & 0 \\ -\omega & 0 & 0 & \frac{1}{C} & 0 \\ -\frac{1}{L} & 0 & -\frac{R}{L} & \omega & 0 \\ 0 & -\frac{1}{L} & -\omega & -\frac{R}{L} & 0 \\ 0 & 0 & \frac{2}{\pi C_{LVS}} & 0 & 0 \end{bmatrix} \begin{bmatrix} V_1 \\ V_2 \\ I_1 \\ I_2 \\ V_{LVS} \end{bmatrix} + \begin{bmatrix} 0 & 0 \\ 0 & 0 \\ \frac{1}{L} & 0 \\ 0 & \frac{1}{L} \\ 0 & 0 \end{bmatrix} \begin{bmatrix} \Delta V_1 \\ \Delta V_2 \end{bmatrix} \tag{2.6}$$

where the new states V_1 and V_2 are the real and imaginary part of the capacitor voltage, and the C term is the capacitance of the resonant capacitor.

2.4 Switching Scheme

The DAB PEC has two H-bridges, which are operated to produce controlled voltages. The operation of these H-bridges requires a switching scheme that is constructed with a high switching frequency, which is set to accommodate the HFT characteristics. Furthermore, the DAB PEC is designed to process ac voltages at certain frequencies, thus the switching frequency has to be maintained constant. Finally, a desired switching scheme for the DAB PEC has to ensure a minimum number of switching actions for both H-bridges. The aforementioned requirements of a desired switching scheme for the DAB PEC can be met by a high frequency square-wave switching scheme. Since the DAB is operated to produce voltages with different magnitudes and controlled phase-shifts, durations and locations of switching pulses (applied to both H-bridges) have to be controlled.

Figure 2.4 shows the effects of controlling the locations and durations of the switching pulses used to operate both H-bridges. The control of the durations of switching pulses is achieved by adjusting d_p and d_s, while the control of switching pulses locations is achieved by adjusting d_θ. The effects of adjusting d_p, d_s, and d_θ on ΔV (see equations (2.1) and (2.6)) can be quantified by determining the real and imaginary components of the ac voltage waveform. The real and imaginary components of the ac voltage can be determined by converting d_p and d_s waveform magnitudes, along with converting d_θ into the phase angle of the primary side voltage $\bar{V}_P$. It should be noted that the phase angle of $\bar{V}_P$ is measured in reference to the secondary side

voltage V_S.

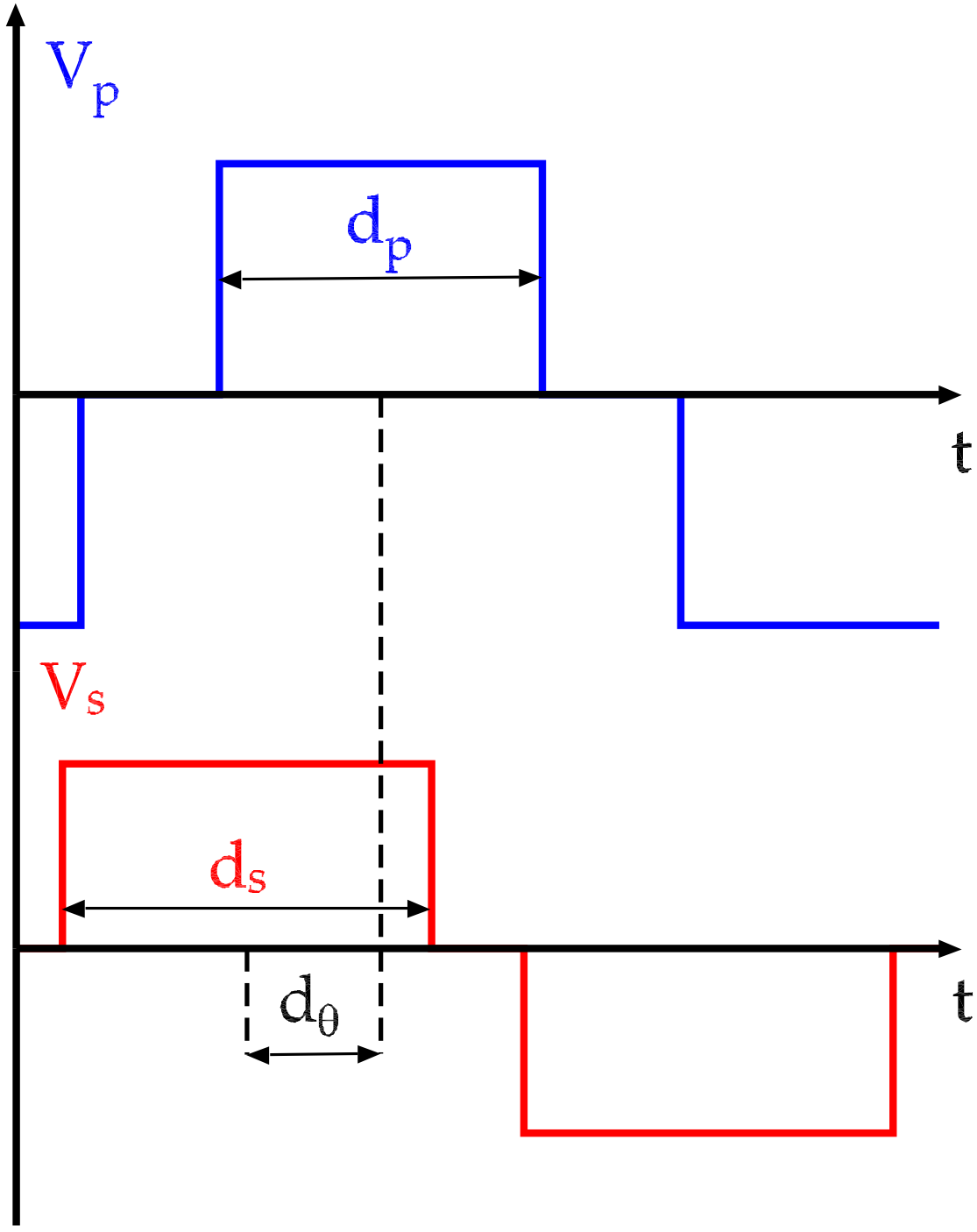

Figure 2.4: Sample waveforms for V_P and V_S over one cycle of operating the DAB PEC. The notation d_p denotes the duty cycle of V_p, d_s denotes the duty cycle of V_S, and d_θ denotes to the phase shift between V_p and V_s.

For purposes of demonstrating the functionality of the switching scheme, a simulation for the open loop operation of the DAB PEC is conducted. This simulation test is conducted with $d_p = 0.8\pi$, $d_s = \pi$, and $d_\theta = -0.2$. Figure 2.5 shows the simulated primary and secondary sides voltages of the HFT. Moreover, Figure 2.6 shows the currents flowing through the medium and low voltages sides of the DAB PEC, along with the current flowing through the HFT.

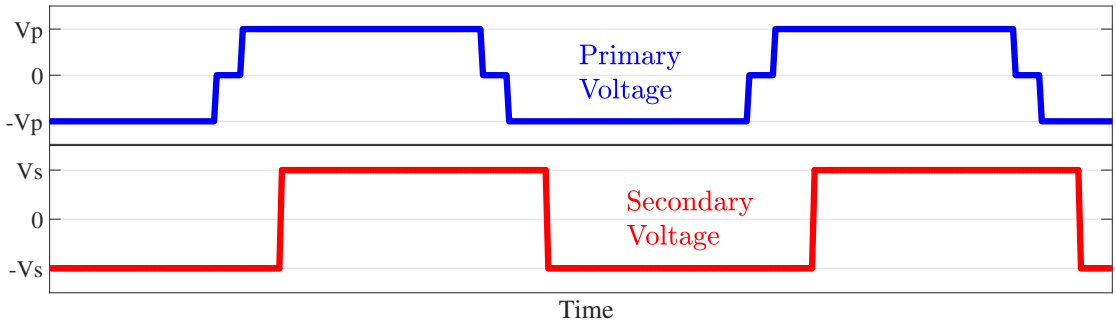

Figure 2.5: The simulated open-loop operation of the DAB PEC: the primary side and secondary sides voltages.

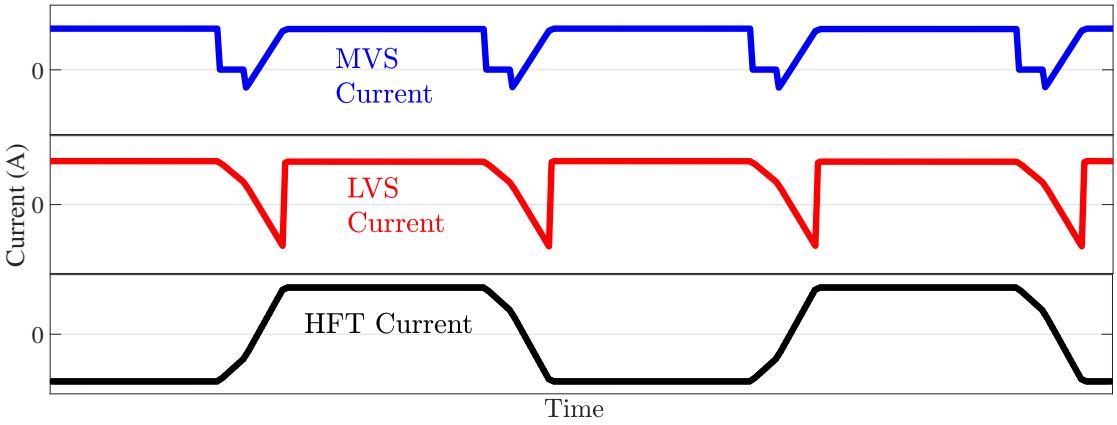

Figure 2.6: The simulated open-loop operation of the DAB PEC: the currents flowing on the medium and low voltage sides of the HFT, along with the current flowing through the HFT itself.

The results in Figure 2.5 and Figure 2.6 show that a non-zero phase shift between the primary and secondary side voltages ensures the flow of a current in the HFT. The HFT current has a zero average value, which implies that both sides of the trans-

former will have currents. These currents will flow through the switching elements of the DAB (as seen from the MVS and LVS currents). It should be noted that the harmonic contents in MVS and LVS currents will flow through the capacitors on both sides of the DAB PEC. As a result, the currents flowing through the front ends of the DAB PEC will be free from the dips seen in MVS and LVS currents (Figure 2.6).

2.4.1 Including the Switching Scheme in the State-Space Model of the DAB PEC

The Fourier series can be applied to the waveforms in Figure 2.4 in order to relate the amplitudes of V_P and V_S to d_p and d_s. The Fourier series of $V_P(t)$ and $V_S(t)$ can be stated as:

$$V_P(t) = V_{MVS} \sum_{n=1,3,..}^{\infty} \left(\frac{4}{n\pi} \sin\left(\frac{nd_p}{2}\right) \sin\left(n\Omega t - n\pi d_\theta\right) \right) \tag{2.7}$$

$$V_S(t) = V_{LVS} \sum_{n=1,3,..}^{\infty} \left(\frac{4}{n\pi} \sin\left(\frac{nd_s}{2}\right) \sin(n\Omega t) \right) \tag{2.8}$$

Considering only the fundamental components of $V_P(t)$ and $V_S(t)$, that are:

$$\left(V_P\right)_{n=1}(t) = V_{MVS} \frac{4}{\pi} \sin\left(\frac{d_p}{2}\right) \sin\left(\Omega t - \pi d_\theta\right) \tag{2.9}$$

$$\left(V_S\right)_{n=1}(t) = V_{LVS} \frac{4}{\pi} \sin\left(\frac{d_s}{2}\right) \sin(n\Omega t) \tag{2.10}$$

where $d_p \in [0, \pi]$, $d_s \in [0, \pi]$, and $d_\theta \in [-1, 1]$. Let $m_p,\ m_s$, and θ be defined as:

$$m_p = \frac{4}{\pi} \sin\left(\frac{d_p}{2}\right) \tag{2.11}$$

$$m_s = \frac{4}{\pi} \sin\left(\frac{d_s}{2}\right) \tag{2.12}$$

$$\theta = -\pi d_\theta \tag{2.13}$$

The definitions of $m_p,\ m_s$, and θ allows their incorporation into the expressions for ΔV_1 and ΔV_2 as:

$$\Delta V_1 = V_{MVS} m_p \cos(\theta) - V_{LVS} m_s \tag{2.14}$$

$$\Delta V_2 = V_{MVS} m_p \sin(\theta) \tag{2.15}$$

The operation and control of the DAB PEC can create several combinations for converting ΔV_1 and ΔV_2 into their respective $m_p,\ m_s$, and θ. In order to reduce the number of possible combinations to the desired ones, each command value of ΔV_1 and ΔV_2 has to produce one combination of $m_p,\ m_s$, and θ. The linear model of the DAB PEC employs the assumption of $d_s = \pi$, which is translated into imposing limits on the control actions initiated by any controller operating the DAB PEC. These two conflicting requirements can be balanced by structuring the controller operation to maintain $d_s = \pi$ as long as it does not contradict the control actions to regulate ΔV_1 and ΔV_2.

2.5 Summary

This chapter has presented structures for the conventional and resonant dual bridge active (DAB) dc-dc power electronic converters (PECs). Both designs of the DAB PECs employ a high frequency transformer (HFT) to provide isolation between both sides of the dc-dc PEC. This chapter has also presented a state-space model for DAB PECs. The presented state-space model has been derived based on assumptions, which have facilitated the linearization of the final model. The obtained linear state-space model for the DAB PEC has been further manipulated to include a switching scheme that is responsible for operating the switching elements on both sides of the HFT. The desired switching scheme has been designed as a square-wave switching, and has been constructed to have its inputs as d_p, d_s, and d_θ. The control actions to regulate ΔV_1 and ΔV_2 have been converted into respective values of d_p, d_s, and d_θ, which are required as inputs for the switching scheme. Finally, the derived linear state-space model in this chapter can be suitable for designing a controller to operate the DAB PEC under different operating conditions. The next chapter presents the development and testing of a linear quadratic regulator (LQR) for the DAB PECs.

Chapter 3

State Feedback Control for DAB PEC

3.1 General

The previous chapter has introduced the DAB PEC as an isolated bi-directional dc-dc PEC, which can be deployed in systems that required active dc-links. Chapter 2 has also developed steady-state modeling for the DAB PEC, as well as its resonant variant using circuit models that have been characterized by state-space mathematical models. The derived state-space models have been linearized with the help of mathematical transformations. The final state-space linear have been tested for open loop steady-state operation, and has demonstrated a good performance. This chapter develops and designs a linear state feedback controller to operate DAB PECs over range of input/output changes.

The main challenge for developing and designing a linear state feedback controller is overcome the limitations on the controllable values of voltage commands ΔV_1 and ΔV_2. The limitations on the controllable values for ΔV_1 and ΔV_2 have been highlighted in equations (2.14) and (2.15), which have linked the command values of ΔV_1 and ΔV_2 with the inputs to the switching scheme to operate the DAB PEC.

This challenge can be addressed by employing a linear-quadratic regulator (LQR), which can operated with limited ranges of control commands.

The design of the desired LQR controller will ensure the ability to operate the DAB PEC as a bi-directional PEC, along with maintaining the isolation between both sides of the high frequency transformer (HFT). These constraints on the design of the LQR controller imply that its responses have to be able to reject disturbances, along with accommodating bi-directional current flows. Finally, the desired LQR is designed to regulate the voltages on the low voltage side of the HFT, with minor sensitivity to the changes in the input voltages, changes in the output power, and changes in component parameters.

3.2 Linear Quadratic Regulator

3.2.1 LQR Model

The linear-quadratic regulator (LQR) is a linear state feedback controller that functions by considering all states of the controlled system. The main concept of the LQR operation is to regulate all states of the controlled systems in order to optimize the system response, and ensure accurate, dynamic, and stable system performance. In general, the optimization of system response is achieved by minimizing a cost function, which is formulated in terms of system states and inputs. System states are expressed using the state cost matrix Q, which assigns a weight for each system state, thus prioritizing certain states and ignoring other states. System inputs are expressed in terms of the input cost matrix R, which assigns weights to all system

inputs to ensure limits of control inputs are considered in the control responses produced by the LQR. The solution to such an optimization problem is a control law, u, that outputs control actions to operate the controlled system.

The cost function J associated with a LQR can be stated as:

$$J(u) = \int_0^\infty (x^T Q x + u^T R u) dt \tag{3.1}$$

$$u = -Kx \tag{3.2}$$

where x is a vector of system states, Q and R are real diagonal weighting matrices, and K is a gain. The controller output u is the matrix product of K and the states (x) of the system.

The matrices Q and R can be selected based on the maximum deviations of all states. Let $m_1, m_2, \ldots, m_n$ be the maximum deviations of the n states of a system, and $\nu_1, \nu_2, \ldots, \nu_n$ be the maximum deviations in the inputs, the Q and R can be selected as:

$$Q = \begin{bmatrix} \left(\frac{1}{m_1}\right)^2 & 0 & \ldots & 0 \\ 0 & \left(\frac{1}{m_2}\right)^2 & \ldots & 0 \\ \vdots & \vdots & \vdots & \vdots \\ 0 & 0 & \ldots & \left(\frac{1}{m_n}\right)^2 \end{bmatrix} \tag{3.3}$$

$$R = \begin{bmatrix} \left(\frac{1}{\nu_1}\right)^2 & 0 & \dots & 0 \\ 0 & \left(\frac{1}{\nu_2}\right)^2 & \dots & 0 \\ \vdots & \vdots & \vdots & \vdots \\ 0 & 0 & \dots & \left(\frac{1}{\nu_n}\right)^2 \end{bmatrix} \tag{3.4}$$

3.2.2 Integral Action

Similar to other state feedback controllers, the LQR function can be improved by accurate modeling of the controlled system. However, the accuracy of modeling certain systems may not be fully achieved due to:

i) some system components may have complex models, non-linear models, and/or validity over limited range of operating conditions;

ii) some system components can have tolerances that can lead errors in their modeling;

iii) some system components can have their characteristics change as they age.

In order to accommodate such sources of model inaccuracies an integral action is typically added to state feedback controllers.

The inclusion of an integral action in a LQR can be accomplished by introducing an artificial state, $\mathcal{V}$. The state $\mathcal{V}$ can be defined as:

$$\frac{d\mathcal{V}}{dt} = V_{LVS} - V_{LVSd} \tag{3.5}$$

where V_{LVSd} is the reference voltage. The introduced state $\mathcal{V}$ has to be included in

the state matrix A of the state space model for the controlled system. The addition of the state $\mathcal{V}$ ensures that the desired LQR will initiate its actions, and will achieve a minor steady-state error.

3.3 LQR for DAB PEC

The previous section has discussed the structure of the LQR, along with the addition of an integral action. In order to structure a LQR for a DAB PEC, this section discusses the tuning requirements to ensure accurate and dynamic LQR responses to operate a DAB PEC.

3.3.1 Tuning the LQR

The design of a LQR mandates obtaining the matrices of maximum deviations, Q and R. For a DAB PEC, the matrices Q and R are determined based on the following settings:

i) The deviation in V_{LVS} is set to be less than 10% of the nominal value. This deviation is set to avoid tripping voltage-based protective devices.

ii) The deviation in I_1 is set to be 5x the rated current of the DAB PEC.

iii) The deviation in I_2 is set to be 5x of the rated current of the DAB PEC. While a deviation value of 0 would be ideal, it should not be too low to interfere with voltage regulation of the low voltage side.

iv) The deviation in $\mathcal{V}$ is based on the deviation in V_{LVS} and the time constant of the HFT.

v) The deviation in ΔV_1 and ΔV_2 are set to be $\frac{4}{\pi}$ times the system voltage V_{SYS}.

The implementation of a LQR involves measuring voltages and currents, which may experience noise or delays. Furthermore, measured quantities can have additional errors caused by variations in component parameters. Such errors may impact the stability of the desired LQR, thus deteriorating the operation of the DAB PEC. These concerns can be mitigated by relaxing the maximum deviations used to determine the Q and R matrices.

3.3.2 The Structure of the Designed LQR

The developed state-space model for the DAB PEC has been used to design a LQR. The structure of the DAB with the designed LQR is illustrated in the block diagram shown in Figure 3.1. This structure sets the control command U as a scaled version (by the gain K) of the difference between the *Reference* and output states. Setting the matrices $A,\ B,\ X$ to have the variables of the state-space model of the DAB PEC (see equation (2.1) in section 2.3, Chapter 2), and incorporating the integral action, the following state-space model can be derived:

$$\begin{bmatrix} \dot{I}_1 \\ \dot{I}_2 \\ \dot{V}_{LVS} \\ \dot{\mathcal{V}} \end{bmatrix} = \begin{bmatrix} -\frac{R}{L} & \omega & 0 & 0 \\ -\omega & -\frac{R}{L} & 0 & 0 \\ \frac{2}{\pi C_{LVS}} & 0 & 0 & 0 \\ 0 & 0 & 1 & 0 \end{bmatrix} \begin{bmatrix} I_1 \\ I_2 \\ V_{LVS} \\ \mathcal{V} \end{bmatrix} + \begin{bmatrix} \frac{1}{L} & 0 \\ 0 & \frac{1}{L} \\ 0 & 0 \\ 0 & 0 \end{bmatrix} \begin{bmatrix} \Delta V_1 \\ \Delta V_2 \end{bmatrix} \tag{3.6}$$

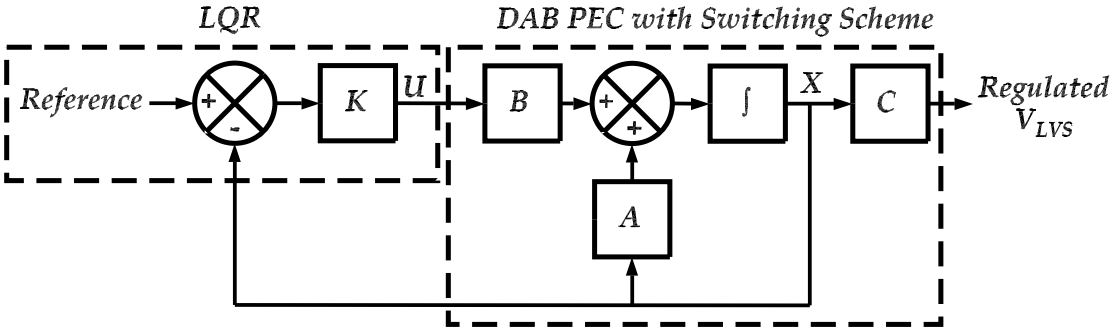

Figure 3.1: Control system block diagram of the DAB PEC system with its LQR

The block representing the *DAB PEC with Switching Scheme*, Figure 3.1, has to be further manipulated in order to ensure translating the controller commands ΔV_1 and ΔV_2 into commands for the switching signals. Such a manipulation of this block is carried out as in the following steps:

a) the measured currents on both sides of the HFT are converted into the states I_1 and I_2;

b) feedback gains of the designed LQR are applied to the states in order to determine command values for ΔV_1 and ΔV_2;

c) ΔV_1 and ΔV_2 are converted into $d_p,\ d_s$, and d_θ using V_{LVS} and V_{MVS}.

The outcome of the aforementioned manipulation stages are depicted in Figure 3.2.

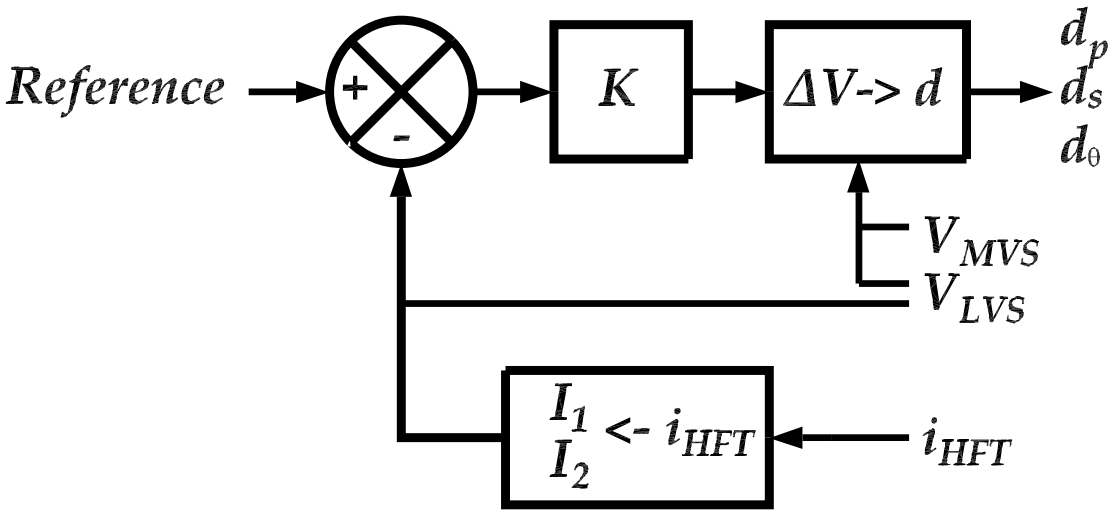

Figure 3.2: Block Diagram of the DAB PEC controller with sensor inputs and switching scheme command outputs

3.4 Summary

This chapter has presented the design and structure for a state feedback controller for operating DAB PECs. The designed state feedback controller has been an LQR that has been tuned to regulate the voltage on the low voltage side of the DAB PEC and reduce imaginary current in the HFT. The tuning of the desired LQR has been initially carried out using the classical tuning approach. In a later stage, the LQR tuning has been modified to accommodate the practical implementation of the DAB PEC and LQR. In addition, an integral action has been included in the final design of the LQR in order to minimize possible steady state errors. The next chapter, Chapter 4, presents the implementation of the tested DAB PEC, along with the designed LQR. It also presents and discuses test results under different operating and loading conditions.

Chapter 4

Performance of the LQR Based Controller

4.1 General

In the previous chapters, linear models have been developed for conventional and resonant DAB PECs. These models have been used to design and tune LQR controllers to regulate input and output voltages and currents. The designed LQR controllers have been featured with integral actions, which are responsible for correcting steady-state errors and maintaining the accuracy of the LQR control actions. Furthermore, the turning of the designed LQR controllers has been carried to ensure their responsiveness and stability during changes in operating conditions. This chapter presents and discusses the performance testing of the developed LQR controllers for operating DAB PECs under different conditions. Test cases presented in this chapter are focused on the ability of the controller to maintain desired voltage levels under load changes, supply disturbances, and reverse power flow. Finally, Chapter 4 provides a performance comparison between the designed LQR and conventional proportional-integral (PI) controllers, when operating DAB and resonant DAB PECs.

4.2 Simulation Model

The performance of the designed LQR controllers was evaluated through simulation tests, which were conducted using models constructed in the MATLAB/SIMULINK software. The parameters for the constructed models are determined first, then they were integrated as parts of these models.

4.2.1 Determining Parameters of LQR Controllers

The first stage of the performance testing was to tune the designed LQR controllers by obtaining values for the matrices Q and R, then calculating numerical values for the matrix K. These calculations were conducted using a MATLAB code, using the following equations for the Q and R matrices:

$$Q = \begin{bmatrix} {q_1}^2 & 0 & 0 & 0 \\ 0 & {q_2}^2 & 0 & 0 \\ 0 & 0 & {q_3}^2 & 0 \\ 0 & 0 & 0 & {q_4}^2 \end{bmatrix} \tag{4.1}$$

where:

$$q_1 = \frac{1}{5\, I_{Rated}} \tag{4.2}$$

$$q_2 = \frac{1}{5\, I_{Rated}} \tag{4.3}$$

$$q_3 = \frac{1}{0.05\, V_{LVSd}} \tag{4.4}$$

$$q_4 = \frac{1}{0.05\, V_{LVSd}\, \frac{L}{R}} \tag{4.5}$$

$$R = \begin{bmatrix} r^2 & 0 \\ 0 & r^2 \end{bmatrix} \tag{4.6}$$

where:

$$r = \frac{1}{V_{SYS}\, \frac{4}{\pi}} \tag{4.7}$$

For the resonant DAB PEC, a similar method was employed to calculate the LQR parameters. However, few adjustments were made by increasing the maximum deviation for I_2 (to improve the stability), and reducing the maximum deviation for $\mathcal{V}$ (to reduce the settling time). It should be noted that these adjustments were needed due to the nature of the resonant DAB PEC being slower than the conventional DAB PEC. The calculations of Q_{res} were carried out with setting values for V_1 and V_2 to zero, as the values of V_1 and V_2 were related to the values of I_1 and I_2. The matrices Q_{res} and R_{res} were determined as:

$$Q_{res} = \begin{bmatrix} 0 & 0 & 0 & 0 & 0 & 0 \\ 0 & 0 & 0 & 0 & 0 & 0 \\ 0 & 0 & q_1^2 & 0 & 0 & 0 \\ 0 & 0 & 0 & q_2^2 & 0 & 0 \\ 0 & 0 & 0 & 0 & q_3^2 & 0 \\ 0 & 0 & 0 & 0 & 0 & q_4^2 \end{bmatrix} \tag{4.8}$$

where:

$$q_1 = \frac{1}{5\ I_{Rated}} \tag{4.9}$$

$$q_2 = \frac{1}{10\ I_{Rated}} \tag{4.10}$$

$$q_3 = \frac{1}{0.05\ V_{LVSd}} \tag{4.11}$$

$$q_4 = \frac{1}{0.05\ V_{LVSd}\ \frac{L}{2R}} \tag{4.12}$$

$$R_{res} = \begin{bmatrix} r^2 & 0 \\ 0 & r^2 \end{bmatrix} \tag{4.13}$$

where:

$$r = \frac{1}{V_{SYS}\ \frac{4}{\pi}} \tag{4.14}$$

The determined parameters for both LQR controllers were used as part of SIMULINK models that were constructed for the DAB and resonant DAP PECs. These models are discussed in the next subsection.

4.2.2 Constructed Models for the DAB and Resonant DAB

Two models were constructed using MATLAB/SIMULINK software. The first model was for a conventional DAB PEC, while the second model was for a resonant DAB PEC. The two models were constructed using the data listed in Table 4.1.

Table 4.1: Data for the Constructed SIMULINK models of the Conventional and Resonant DAB PECs

Parameter	Value	Unit
System voltage (V_{SYS})	360	$[V]$
Desired V_{LVS} (V_{LVSd})	360	$[V]$
Rated load	250	$[W]$
Rated current	0.69	$[A]$
HFT resistance (R)	0.1	$[\Omega]$
HFT inductance (L)	400	$[\mu H]$
Resonant capacitance (C)	12.9	$[nF]$
LVS capacitance (C_{LVS})	40	$[\mu F]$
System frequency	70	$[kHz]$
Simulation time step (T_s)	35.7	$[ns]$

The data in Table 4.1 was used to calculate numerical values for the matrices Q, R, Q_{res}, and R_{res}. Once the matrices Q and R were determined, the numerical values for the matrix K were calculated to be as provided in equation (4.15):

$$K = \begin{bmatrix} 132.4 & 0.3633 & 17.51 & 3838 \\ 0.3633 & 132.6 & 23.19 & 5079 \end{bmatrix} \tag{4.15}$$

Similarly, the matrices Q_{res} and R_{res} were used to calculate numerical values for the matrix K_{res}. The numerical values for the matrix K_{res} were calculated to be as:

$$K_{res} = \begin{bmatrix} -0.0279 & -0.0797 & 120.6 & 4.2813 & 29.80 & 1273 \\ -0.1010 & 0.0190 & 4.281 & 83.80 & 0.1974 & 86.51 \end{bmatrix} \tag{4.16}$$

4.3 Simulated Performance

4.3.1 DAB Performance Tests

4.3.1.1 Steady-State Operation

The first test of the designed LQR aimed to demonstrate its performance during steady-state operation. This test was conducted as the constructed conventional DAB supplied a load with 120 W, at a voltage of 360 V. Figure 4.1 shows the waveforms of the two currents I_1 and I_2, reference and actual voltage on the low voltage side of the HFT, and voltage commands ΔV_1 and ΔV_2 for this test.

The results in Figure 4.1 show that actions of the designed LQR controller were successful in maintaining a close match between the reference and actual voltage on the load side. Actions of the designed controller were also effective in maintaining a small value for I_2, while providing a high quality current to the load (I_1 without oscillations or spikes). The results of the first test revealed promising ability of the designed LQR to operate the DAB to meet the reference voltage, while minimizing I_2.

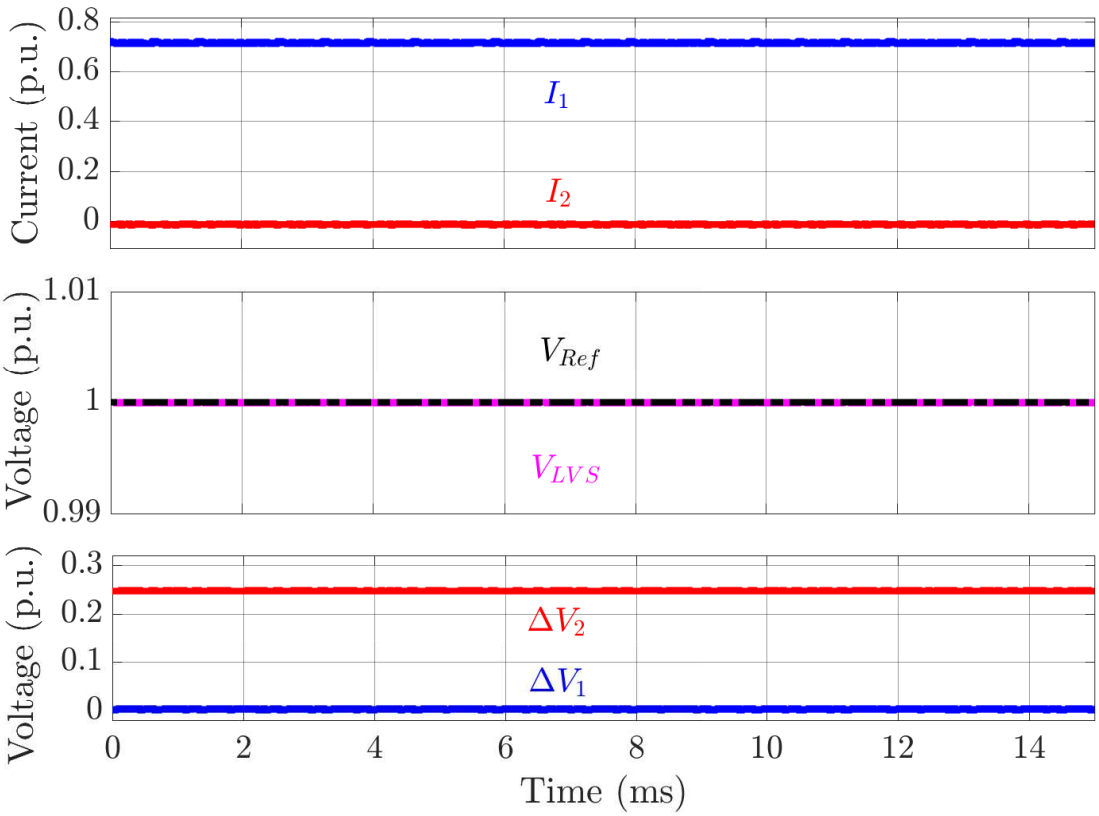

Figure 4.1: The steady-state responses of the conventional DAB PEC with the designed LQR controller. The per-unit currents I_1 and I_2 (base current is 0.69 A), per-unit reference and actual voltage on the low voltage side of the HFT (base voltage is 360 V), and per-unit voltage commands ΔV_1 and ΔV_2 (base voltage is 360 V).

4.3.1.2 Step Changes in Load Power Demands

The second test was step changes in the power demands fed by the DAB PEC. This test aimed to evaluate the performance of the designed LQR controller for changes in the load power demands, while the conventional DAB PEC operated as a bi-directional PEC. The step changes in the load power demands were created at $V_{LVS} = 360V$, and they were set as:

$$P_L = 0 \rightarrow 80 \rightarrow 250 \rightarrow -250 \rightarrow 250W \tag{4.17}$$

Each step changes lasted for 20 ms., and the last step change represented the largest possible change in the load power demands of the designed LQR controller. Figure 4.2 shows the waveforms of the two currents I_1 and I_2, reference and actual voltage on the low voltage side of the HFT, and voltage commands ΔV_1 and ΔV_2 for this test.

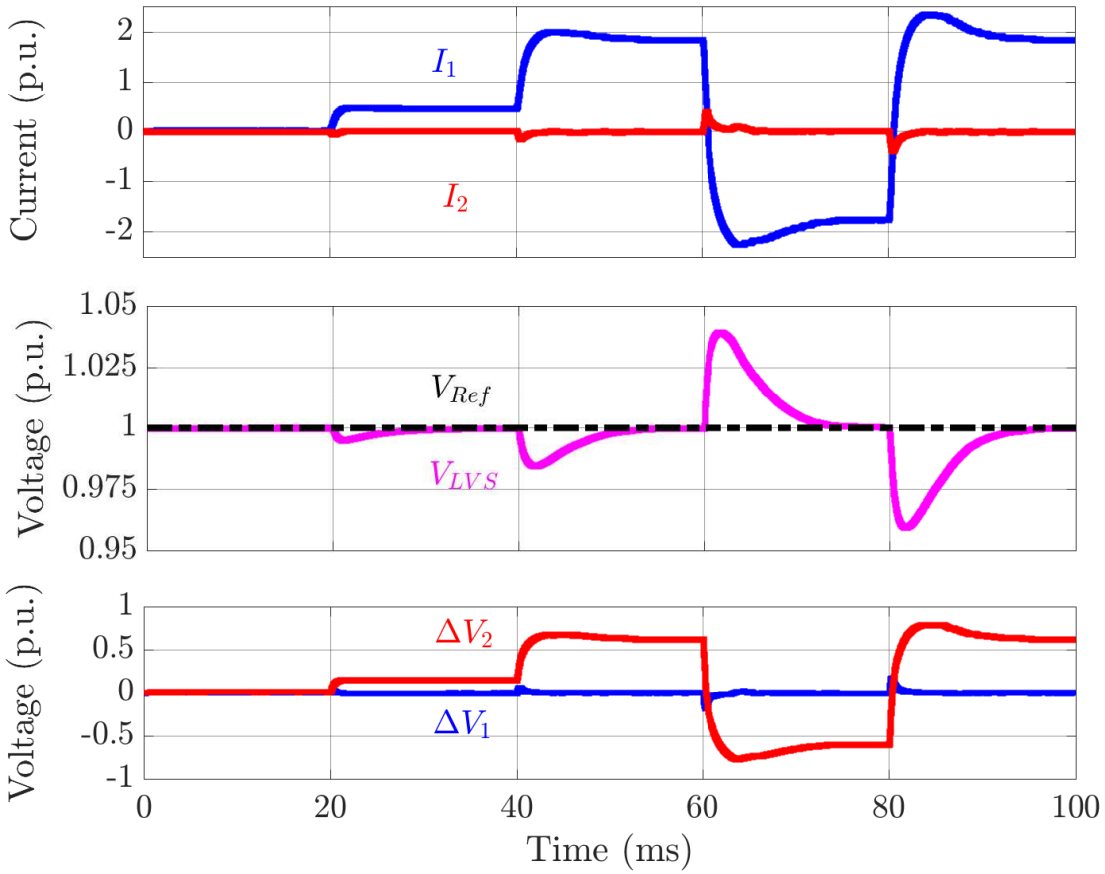

Figure 4.2: Responses of the conventional DAB PEC with the designed LQR controller to step changes in load power demands. The per-unit currents I_1 and I_2 (base current is 0.69 A), per-unit reference and actual voltage on the low voltage side of the HFT (base voltage is 360 V), and per-unit voltage commands ΔV_1 and ΔV_2 (base voltage is 360 V).

It could be seen from Figure 4.2 that the actions of the designed LQR controller were effective in operating the conventional DAB PEC so that minor overshoots were experienced by the current I_1. These actions were also accurate in producing negligible deviations in V_{LVS} from its reference value. In addition, the designed LQR was successful in maintaining a small value of I_2 during and post the step changes in P_L. Finally, actions of the designed LQR controller ensured small deviations in the voltages on both sides of the HFT, as indicated by ΔV_1 and ΔV_2. The results of the second test were in agreement with those obtained from the first test, where the designed LQR was able to operate the conventional DAB PEC and ensure minimum deviations in the voltages and currents on both sides of the HFT. These response features were not affected by the loading level and/or direction of the power flow. It should be noted that equation (3.6) provided a relationship between I_1 and ΔV_2 during dynamic conditions. This relationship could be observed from the results in Figure 4.2.

In order to demonstrate the capabilities of the designed LQR controller, the conventional DAB was operated by a proportional-integral (PI) controller using the single phase shift (designed based on the discussions in references [16] and [19]). The PI controlled DAB PEC was tested with the same changes in P_L. The currents I_1 and I_2, together with the reference and actual voltage on low voltage side of the HFT for this comparison test are shown in Figure 4.3.

The results in Figure 4.3 show that the PI controller was able to limit the deviations in V_{LVS} from its reference value, and limited the overshoot in I_1. However, the PI controller was not able to maintain a low value for I_2 during and post the step changes in P_L. The limited ability of the PI controller in minimizing I_2 could be considered as an advantage of the designed LQR controller, which was successful in

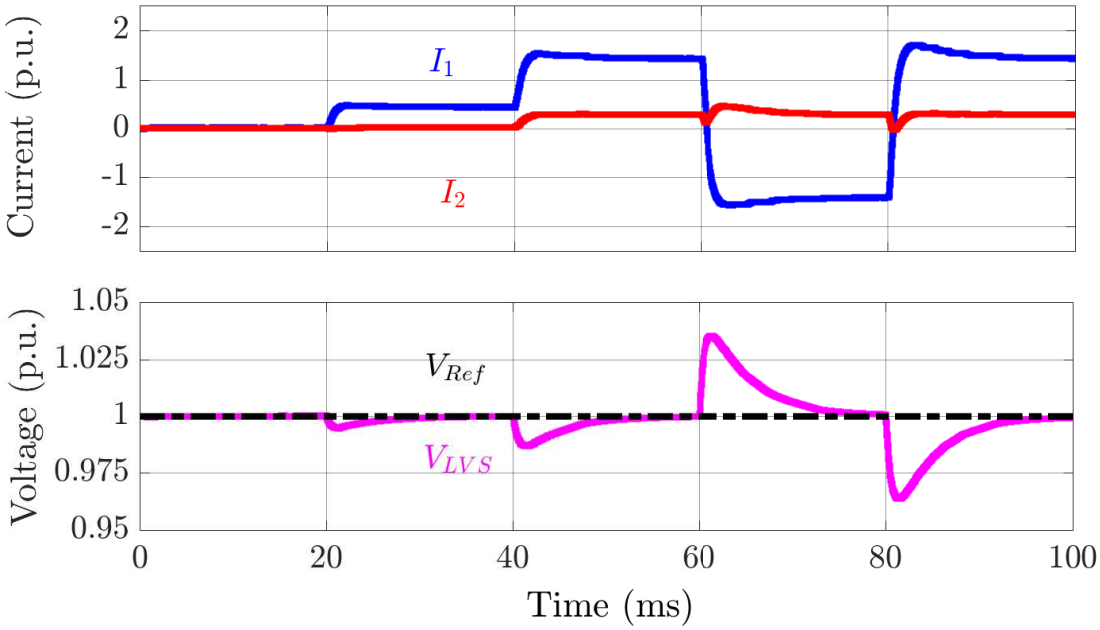

Figure 4.3: Responses of the conventional DAB PEC with a PI controller to step changes in load power demands. The per-unit currents I_1 and I_2 (base current is 0.69 A), per-unit command and actual voltage on the low voltage side of the HFT (base voltage is 360 V), and per-unit voltage commands ΔV_1 and ΔV_2 (base voltage is 360 V).

ensuring a close-to-zero value of I_2 under different loading levels.

4.3.1.3 Step Changes in Supply Voltage

The third test was step changes in the supply voltage (V_{MVS}), which were created as:

$$V_{MVS} = 1 \rightarrow 0.9 \rightarrow 1 \rightarrow 1.1 \rightarrow 1\, p.u. \tag{4.18}$$

Each change in V_{MVS} lasted for 20 ms. It should be noted that the changes in V_{MVS} were set as $\pm 10\%$, which could be real cases for PECs interconnected with a power

system feeder. The third test aimed to examine the responses of the designed LQR controller for changes in V_{MVS} as the load power demands were kept unchanged at $P_L = 200$ W. Figure 4.4 shows the waveforms of the two currents I_1 and I_2, command and actual voltage on the low voltage side of the HFT, and voltage commands ΔV_1 and ΔV_2 for this test.

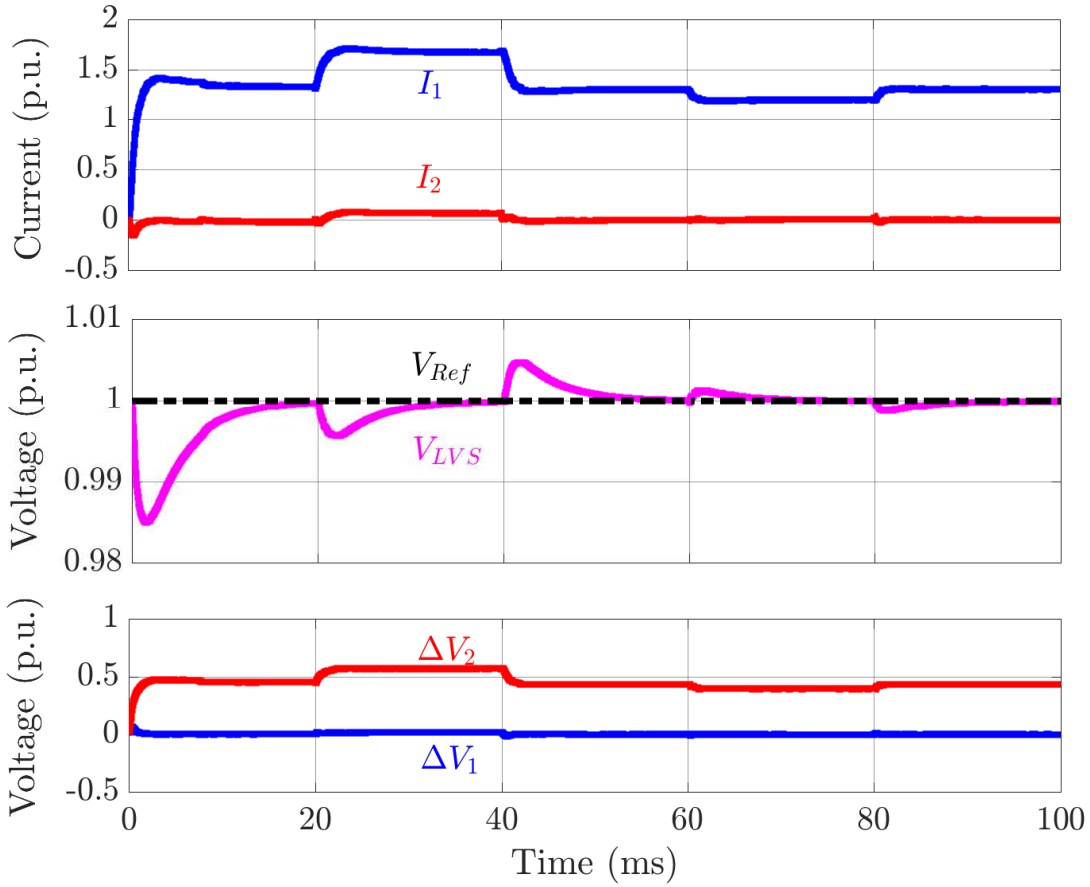

Figure 4.4: Responses of the conventional DAB PEC with the designed LQR controller to step changes in the supply voltage while supporting a 200 W load. The per-unit currents I_1 and I_2 (base current is 0.69 A), per-unit reference and actual voltage on the low voltage side of the HFT (base voltage is 360 V), and per-unit voltage commands ΔV_1 and ΔV_2 (base voltage is 360 V).

Figure 4.4 demonstrates that the actions of the designed LQR controller were able to adjust I_1 in response to changes in V_{MVS} in order to maintain the power demands

of the load. The changes in I_1 were fast, accurate, and with negligible overshoots. Furthermore, actions of the designed LQR were effective in operating the conventional DAB PEC so that minor variations in I_2, along with negligible deviations in V_{LVS} from its command value. Moreover, actions of the designed LQR controller resulted in small deviations in the voltages on both sides of the HFT, as indicated by ΔV_1 and ΔV_2. It should be noted that changes in ΔV_1 and ΔV_2, due to changes in V_{MVS}, were due to their relationship with d_p, d_s, and d_θ. The expressions of ΔV_1 and ΔV_2 in terms of d_p, d_s, and d_θ factored in measured values of V_{MVS}. The results of the third test were in agreement with the results obtained from previous tests, where the designed LQR was able to operate the conventional DAB PEC and ensure minimum deviations in the voltages and currents on both sides of the HFT. Actions of the designed LQR controller were not impacted by the changes in V_{MVS}, loading level and/or direction of the power flow.

4.3.2 Resonant DAB Performance Tests

4.3.2.1 Steady-State Operation

The first test of the LQR controlled resonant DAB PEC was the steady-state test (fixed V_{MVS} and fixed P_L). The objective of this test was to investigate the responses of the designed LQR, when operating a resonant DAB PEC in a steady-state condition. This test was conducted as the resonant DAB PEC supplied a load with 120 W, at a voltage of 360 V. The steady-state test was done with the resonant DAB PEC controller. This test was conducted as the constructed resonant DAB supplied a load with 120 W, at a voltage of 360 V. Figure 4.5 shows the waveforms of the two resonant capacitor voltages V_1 and V_2, two currents I_1 and I_2, reference and actual

voltage on the low voltage side of the HFT, and voltage commands ΔV_1 and ΔV_2 for this test.

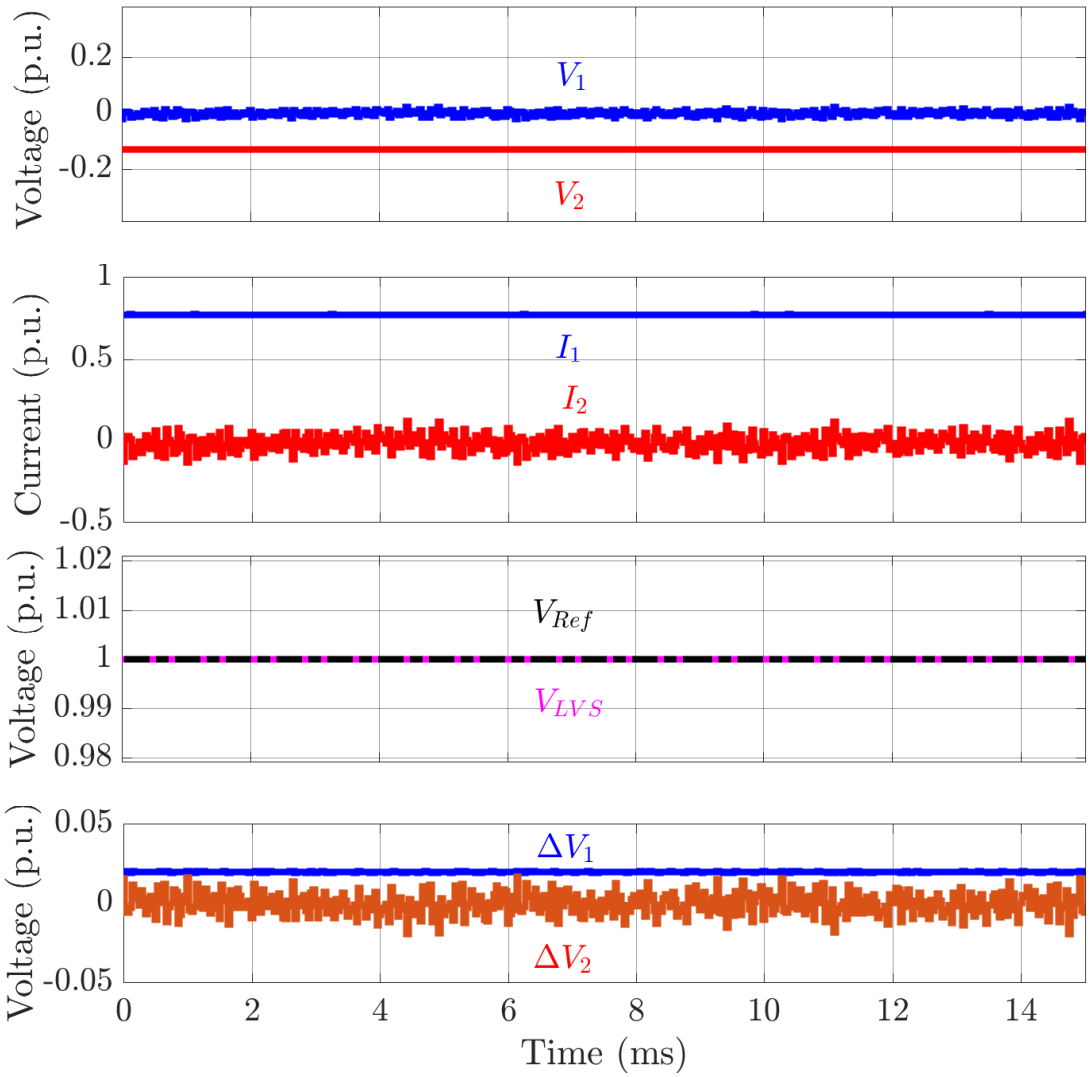

Figure 4.5: The steady-state responses of the resonant DAB PEC with the designed LQR controller. The per-unit currents I_1 and I_2 (base current is 0.69 A), per-unit reference and actual voltage on the low voltage side of the HFT (base voltage is 360 V), and per-unit voltage commands ΔV_1 and ΔV_2 (base voltage is 360 V).

The results in Figure 4.5 show that actions of the designed LQR controller were successful in maintaining a close match between the reference and actual voltage on the load side. Actions of the designed controller were also effective in maintaining a

small value for I_2, which had some ripples that were generated due to the presence of the resonant capacitance C. Despite the ripples in I_2, actions of the designed LQR controller were successful in operation the resonant DAB PEC to produce a stable I_1 (with minor ripples), and with a value much larger than that of I_2. Moreover, actions of the designed controller operated the resonant DAB PEC to maintain a minor deviation in the voltage of the low voltage side from its reference value. The results of the first test revealed promising ability of the designed LQR to operate a resonant DAB to meet the reference voltage and load power demands, while minimizing I_2.

4.3.2.2 Step Changes in Load Power Demands

The second test was conducted with step changes in the power demands of the load fed by the LQR controlled resonant DAB PEC. This test aimed to evaluate the performance of the designed LQR controller for operating a resonant DAB PEC as a bi-directional PEC with step changes in the load power demands. The tested step changes in load power demands were created as:

$$P_L = 0 \rightarrow 80 \rightarrow 250 \rightarrow -250 \rightarrow 250W \tag{4.19}$$

Each created value of P_L was kept for a time interval of 20 ms. The last step change in P_L represented the maximum loading level of the designed LQR controller. Figure 4.6 shows the waveforms of the two voltages V_1 and V_2, the two currents I_1 and I_2, reference and actual voltage on the low voltage side of the HFT, and voltage commands ΔV_1 and ΔV_2 for this test.

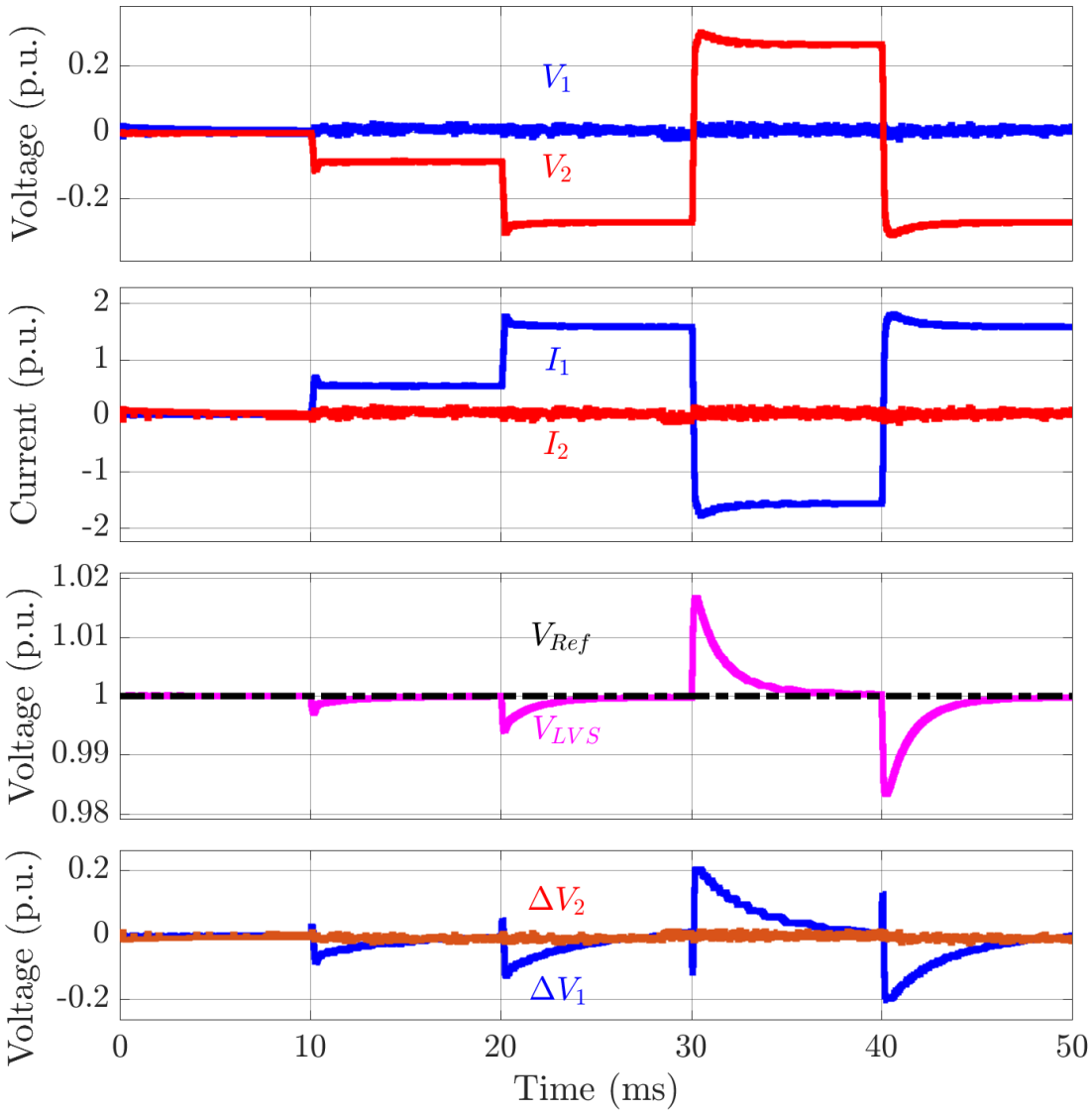

Figure 4.6: Responses of the resonant DAB PEC with the designed LQR controller to step changes in load power demands. The per-unit currents I_1 and I_2 (base current is 0.69 A), per-unit reference and actual voltage on the low voltage side of the HFT (base voltage is 360 V), and per-unit voltage commands ΔV_1 and ΔV_2 (base voltage is 360 V).

It could be seen from Figure 4.6 that the actions of the designed LQR controller were effective in operating the resonant DAB PEC so that minor overshoots were experienced by the current I_1. These actions were also accurate in yielding negligible deviations in V_{LVS} from its reference value. In addition, the designed LQR was

successful in maintaining a small value of I_2 during and post the step changes in P_L. The voltage commands ΔV_1 and ΔV_2 had spikes, which were due to the slow change in the voltage across the resonant capacitor C. The results of the second test were in agreement with the results obtained from the first one, where the designed LQR was able to operate the resonant DAB PEC and ensure minimum deviations in the voltages and currents on both sides of the HFT. These response features were insensitive to loading level and/or direction of the power flow.

4.3.2.3 Step Changes in Supply Voltage

The third test of the LQR controlled resonant DAB PEC was step changes in the supply voltage (V_{MVS}), which were created as:

$$V_{MVS} = 1 \rightarrow 0.9 \rightarrow 1 \rightarrow 1.1 \rightarrow 1\, p.u. \tag{4.20}$$

Each change in V_{MVS} lasted for 20 ms. The objective of this test was to examine the responses of the designed LQR controller for operating a resonant DAB PEC under changes in V_{MVS}, while load power demands were kept unchanged at $P_L = 200$ W. Figure 4.7 shows the waveforms of the voltages V_1 and V_2, currents I_1 and I_2, reference and actual voltage on the low voltage side of the HFT, and voltage commands ΔV_1 and ΔV_2 for this test.

One could see from Figure 4.7 that the actions of the designed LQR controller were able to adjust I_1 in response to changes in V_{MVS} in order to maintain the power demands of the load. The changes in I_1 were fast, accurate, and with negligible overshoots, where impacts of changes in V_{MVS} were mitigated. The actions of the

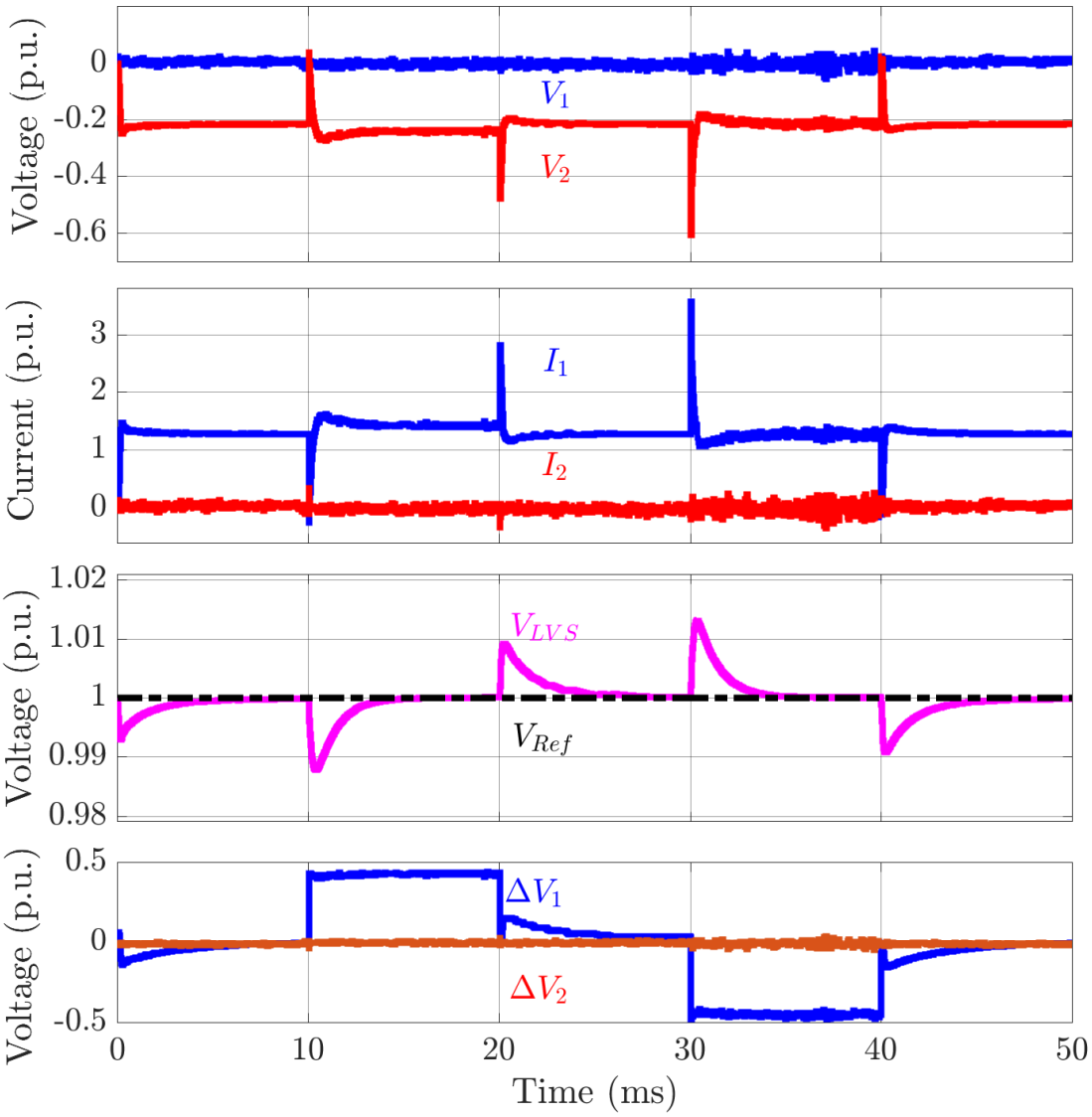

Figure 4.7: Responses of the resonant DAB PEC with the designed LQR controller to step changes in the supply voltage while supporting a 200 W load. The per-unit currents I_1 and I_2 (base current is 0.69 A), per-unit reference and actual voltage on the low voltage side of the HFT (base voltage is 360 V), and per-unit voltage commands ΔV_1 and ΔV_2 (base voltage is 360 V).

designed LQR were effective in operating the resonant DAB PEC minimize the deviations in V_{LVS} from its reference value. It should be noted that the spikes in I_1 and V_2 were due to the presence of the resonant capacitance in series with the HFT. The voltage commands ΔV_1 and ΔV_2 had small variations due to changes in V_{MVS},

which affected d_p, d_s, and d_θ during post changes in V_{MVS}. Finally, actions of the designed LQR was successful in operating the resonant DAB PEC to maintain a small value of I_2 during and post changes in V_{MVS}. The results of the third test were in agreement with the results obtained from previous tests, where the designed LQR was able to operate the resonant DAB PEC and ensure minimum deviations in the voltages and currents on both sides of the HFT. In addition, actions of the designed LQR controller were not impacted by the changes in V_{MVS}, loading level and/or direction of the power flow.

4.4 Summary

This chapter presented test results for the designed LQR controller, when operating conventional and resonant DAB PECs under different conditions. The selection of the LQR parameters has been accurate as has been confirmed by the test results obtained for both DAB PECs. Test results have demonstrated that the designed LQR controllers are capable of operating DAB PECs under changes in load power demands, bi-directional power flow, and changes in the voltage of the medium voltage side. During these tests, the designed LQR controller has shown remarkable capabilities to minimize the ripples in the input/output voltages, deviations in the voltages on both sides of the HFT, overshoots and spikes in voltages and currents on both sides of the HFT, and steady-state errors in all controller states. Furthermore, test results of the designed LQR controller have compared with those obtained using a PI controller under similar operating conditions. Comparison results have shown that the designed controller has similar responses to the PI controller regarding voltage regulation while being able to perform a secondary objective (reducing

imaginary current). Performance and comparison results support the use of the designed LQR controllers for operating conventional and resonant DAB PECs for various applications, including the solid-state power transformers.

Chapter 5

Summary and Conclusions

5.1 Summary

This thesis has presented the design, implementation and performance evaluation of linear quadratic regulator (LQR) controllers for conventional and resonant DAB power electronic converters (PECs). These DAB PECs are widely used in motor drives, power supplies, renewable energy systems, and recently in solid-state power transformers. The design of LQR controllers has been based on developed state-space models for conventional and resonant DAB PECs, where input and output voltages and currents are decomposed into real and imaginary components. These state-space models are quite simple, and have been found to accommodate conventional and resonant DAB PECs. In addition, the developed state-space models have been able to include different states to reflect the switching scheme, which is used to generate switching pulses to operate the switching elements in each DAB PEC.

The designed LQR controllers have been tuned to successfully operate conventional and resonant DAB PECs with various input and output voltages, power ratings, voltage ratios of the high frequency transformers (HFT). Furthermore, the designed LQR controllers have demonstrated encouraging abilities to operate DAB PECs with reduced HFT currents without compromising the voltage control. The features of

the designed LQR controllers have verified through testing under different loading levels, input voltage dynamics, and bi-directional power flows. In these tests, LQR controllers have shown promising performance, which is complemented with minor sensitivity to loading levels and/or direction of power flow.

5.2 Conclusions

This thesis has provided detailed modeling and design of LQR controllers to operate conventional and resonant DAB PECs under different conditions. The objectives of this thesis have been to design and test simple, robust, accurate, and fast controllers for DAB PECs. These objectives have been achieved by the designed LQR controllers, and verified by performance and comparison tests. The following conclusions can be drawn from the research work presented in this thesis:

- Conventional and resonant DAB PECs can be used to implement active and bi-directional dc-links.
- State-space models of conventional and resonant DAB PECs can offer simplified models, and can be modified to include the switching scheme.
- LQR controllers can be a good choice for operating switched systems with multiple inputs and outputs, as well as multiple states.
- The design of LQR controllers can be carried out based on system states and boundaries of inputs and outputs.
- Testing designed LQR controllers have to include different loading levels, dynamics in input voltages, and bi-directional power flow.

5.3 Contributions

The research work presented in this thesis has facilitated making contributions to the operation and control of bi-directional dc-dc PECs. The contributions of this thesis can be summarized as the following:

- The development of a linear state space model for conventional and resonant DAB PECs. This model has shown a good flexibility to include the switching scheme.
- The tuning of an LQR controller based on the boundaries of its inputs and outputs. This tuning process allows operating systems with multiple switched states.
- The design and tuning of LQR controllers to operate systems with multiple switched states, and under dynamics in its inputs.
- The successful testing of LQR controllers for operating conventional and resonant DAB PECs under a wide range of operating conditions.

5.4 Future Work

The successful design and operation of LQR controllers for DAB PECs opens other avenues for future research works. Such works may include:

1. Modifying the switching scheme for LQR-controlled DAB PECs to reduce losses.

2. Including the designed LQR as a sub-controller in the main controller for solid-state transformers.

3. Investigating the applicability of LQR-controlled DAB PECs in grid-connected storage systems.

4. Testing the applicability of the designed LQR controllers for other PECs.

Bibliography

[1] E. R. Ronan, S. D. Sudhoff, S. F. Glover, and D. L. Galloway,"A Power Electronic-Based Distribution Transformer," in *IEEE Transactions on Power Delivery*, Vol. 17, No. 2, pp. 537–543, April 2002

[2] S. Falcones, R. A., and X. Mao,"A DCDC Multiport-Converter-Based Solid-State Transformer Integrating Distributed Generation and Storage," in *IEEE Transactions on Power Electronics*, Vol. 28, No. 5, pp. 2192–2203, May 2013

[3] T. Zhao, G. Wang, S. Bhattacharya, and A. Q. Huang,"Voltage and Power Balance Control for a Cascaded H-Bridge Converter-Based Solid-State Transformer," in *IEEE Transactions on Power Electronics*, Vol. 28, No. 4, pp. 1523–1532, April 2013

[4] L. A. G. Rodriguez, V. Jones, A. R. Oliva, A. Escobar-Meja, and J. C. Balda,"A New SST Topology Comprising Boost Three-Level AC/DC Converters for Applications in Electric Power Distribution Systems," in *IEEE Journal of Emerging and Selected Topics in Power Electronics*, Vol. 5, No. 2, pp. 735–746, June 2017

[5] H. Chen, A. Prasai, R. Moghe, K. Chintakrinda, and D. Divan,"A 50-kVA Three-Phase Solid-State Transformer Based on the Minimal Topology: Dyna-C," in *IEEE Transactions on Power Electronics*, Vol. 31, No. 12, pp. 8126–8137, Dec. 2016

[6] L. F. Costa, G. De Carne, G. Buticchi, and M. Liserre,"The Smart Transformer: A solid-state transformer tailored to provide ancillary services to the distribution

grid," in *IEEE Power Electronics Magazine*, Vol. 4, Is. 12, pp. 56–67, June 2017

[7] X. She, A. Q. Huang, and R. Burgos, "Review of Solid-State Transformer Technologies and Their Application in Power Distribution Systems," in *IEEE Journal of Emerging and Selected Topics in Power Electronics*, Vol. 1, No. 3, pp. 186–198, Sept. 2013

[8] R. W. De Doncker, D. M. Divan, and M. H. Kheraluwala,"A Three-phase Soft-Switched High-Power-Density dc/dc Converter for High-Power Applications," in *IEEE Transactions on Industry Applications*, Vol. 27, No. 1, pp. 63–73, Jan. 1991

[9] M. H. Kheraluwala, R. W. Gascoigne, D. M. Divan, and E. D. Baumann, "Performance Characterization of a High-Power Dual Active Bridge dc-to-dc Converter," in *IEEE Transactions on Industry Applications*, Vol. 28, No. 6, pp. 1294–1301, Nov./Dec. 1992

[10] B. Zhao, Q. Song, and W. Liu,"Efficiency Characterization and Optimization of Isolated Bidirectional DCDC Converter Based on Dual-Phase-Shift Control for DC Distribution Application," in *IEEE Transactions on Power Electronics*, Vol. 280, No. 4, pp. 1711–1727, April 2013

[11] H. Bai and C. Mi,"Eliminate Reactive Power and Increase System Efficiency of Isolated Bidirectional Dual-Active-Bridge DCDC Converters Using Novel Dual-Phase-Shift Control," in *IEEE Transactions on Power Electronics*, Vol. 23, No. 6, pp. 2905–2194, Nov. 2008

[12] B. Zhao, Q. Song, W. Liu, and Y. Sun,"Overview of Dual-Active-Bridge Isolated Bidirectional DCDC Converter for High-Frequency-Link Power-Conversion

System," in *IEEE Transactions on Power Electronics*, Vol. 29, No. 8, pp. 4091–4106, Aug. 2014

[13] W. Choi, K.-M. Rho, and B.-H. Cho,"Fundamental Duty Modulation of Dual-Active-Bridge Converter for Wide-Range Operation," in *IEEE Transactions on Power Electronics*, Vol. 31, No. 6, pp. 4048–4064, June 2016

[14] D.-D. Nguyen, G. Fujita, and M. C. Ta,"Reduced-Order Observer-Based Control System for Dual-Active-Bridge DC/DC Converter," in *IEEE Transactions on Industry Applications*, Vol. 54, No. 4, pp. 3426–3439, July/Aug. 2018

[15] S.-K. Kim and K.-B. Lee,"Robust Feedback-Linearizing Output Voltage Regulator for DC/DC Boost Converter," in *IEEE Transactions on Industrial Electronics*, Vol. 62, No. 11, pp. 7127–7135, Nov. 2015

[16] H. Qin and J. W. Kimball,"Closed-Loop Control of DCDC Dual-Active-Bridge Converters Driving Single-Phase Inverters," in *IEEE Transactions on Power Electronics*, Vol. 29, No. 2, pp. 1006–1017, Feb. 2014

[17] K. M. Yoo and J. Y. Lee, "A 10-kW Two-Stage Isolated/Bidirectional DC/DC Converter With Hybrid-Switching Technique," in *IEEE Transactions on Industrial Electronics*, Vol. 60, No. 6, pp. 2205–2213, June 2013

[18] S.-C. Tan, Y. M. Lai, and C. K. Tse,"General Design Issues of Sliding-Mode Controllers in DCDC Converters," in *IEEE Transactions on Industrial Electronics*, Vol. 55, No. 3, pp. 1160–1174, March 2008

[19] P. Mattavelli, L. Rossetto, G. Spiazzi, and P. Tenti,"General-Purpose Fuzzy Controller for DCDC Converters," in *IEEE TRANSACTIONS ON POWER ELECTRONICS*, Vol. 12, No. 1, pp. 79–86, Jan. 1997

[20] C. Olalla, R. Leyva, A. El Aroudi, and I. Queinnec,"Robust LQR Control for PWM Converters: An LMI Approach," in *IEEE Transactions on Industrial Electronics*, Vol. 56, No. 7, pp. 2548–2558, July 2009

[21] F. H. F. Leung, P. K. S. Tam, and C. K. Li,"The Control of Switching dc-dc Converters -A General LQR Problem," in *IEEE Transactions on Industrial Electronics*, Vol. 38, No. 1, pp. 65–71, Feb. 1991

[22] J. A. Mueller and J. W. Kimball,"An Improved Generalized Average Model of DCDC Dual Active Bridge Converters," in *IEEE Transactions on Power Electronics*, Vol. 33, No. 12, pp. 9975–9987, Nov. 2018

[23] C. Liu, H. Liu, G. Cai, S. Cui, H. Liu, and H. Yao,"Novel Hybrid LLC Resonant and DAB Linear DCDC Converter: Average Model and Experimental Verification," in *IEEE Transactions on Industrial Electronics*, Vol. 64, No. 9, pp. 6970–6978, Sept. 2018

[24] M. Forouzesh, Y. P. Siwakoti, S. A. Gorji, F. Blaabjerg, and B. Lehman,"Step-Up DCDC Converters: A Comprehensive Review of Voltage-Boosting Techniques, Topologies, and Applications," in *IEEE Transactions on Power Electronics*, Vol. 32, No. 12, pp. 9143–9177, Dec. 2017

[25] J. G. Ziegler and N. B. Nichols,"Optimum Settings for Automatic Controllers," in *ASME Journal of Dynamic Systems, Measurement, and Control*, Vol. 115, pp. 220–222, June 1993

[26] B. D. Tyreus and W. L. Luyben,"Tuning PI Controllers for Integrator/Dead Time Processes," in *Industrial & Engineering Chemistry Research*, Vol. 31, No. 11, pp. 2625–2628, Nov. 1992

[27] K. J. Astrom and T. Hagglung,"Automatic Tuning of Simple Regulators," in *IFAC Proceedings Volumes*, Vol. 17, Is. 2, pp. 1867-1872, July 1984

[28] B. Zhao, Q. Song, J. Li, X. Xu, W. Liu,"Comparative Analysis of Multilevel-High-Frequency-Link and Multilevel-DC-Link DCDC Transformers Based on MMC and Dual-Active Bridge for MVDC Application," in *IEEE Transactions on Power Electronics*, Vol. 33, No. 3, pp. 2035–2049, March 2018

[29] S. A. Gorji, H. G. Sahebi, M. Ektesabi, and A. B. Raf,"Topologies and Control Schemes of Bidirectional DCDC Power Converters: An Overview," in *IEEE Access*, Vol. 7, pp. 117997–118019, Aug. 2019

[30] X. Li and A. K. S. Bhat,"Analysis and Design of High-Frequency Isolated Dual-Bridge Series Resonant DC/DC Converter," in *IEEE Transactions on Power Electronics*, Vol. 25, No. 4, pp. 850–862, April 2010

[31] J.-H. Jung, H.-S. Kim, M.-H. Ryu, and J.-W. Baek,"Design Methodology of Bidirectional CLLC Resonant Converter for High-Frequency Isolation of DC Distribution Systems," in *IEEE Transactions on Power Electronics*, Vol. 28, No. 4, pp. 1741–1755, April 2013

Appendix A

Additional Test Cases

Test cases presented in Chapter 4 have demonstrated good performance of the designed LQR controllers to operate conventional and resonant DAB PECs under different conditions. This Appendix provides additional test cases for the designed LQR controllers to operate DAB PECs with different voltage and power ratings. The additional test cases in Appendix A aim to achieve two objectives, which are:

i) extending the the applicability of tunning LQR controllers to other voltage and power ratings;

ii) extending the functionality of the designed LQR controllers to operate parallel-connected DAB PECs (for high input/output powers).

A.1 DAB PEC with Different Ratings

A model for a conventional DAB PEC model was constructed using MATLAB SIMULINK software using the parameters listed in Table A.1. The tunning of the deigned LQR was carried using equations (4.1) and (4.6). The developed model was tested for changes in load power demands, as well as changes in the voltage supplied to the medium voltage side of the DAB PEC.

Table A.1: Parameters of the DAB PEC Model

Parameter	Value	Unit
System voltage (V_{SYS})	660	$[V]$
Desired V_{LVS} (V_{LVSd})	660	$[V]$
Rated load	3300	$[W]$
Rated current	5	$[A]$
HFT resistance (R)	0.1	$[\Omega]$
HFT inductance (L)	100	$[\mu H]$
LVS capacitance (C_{LVS})	40	$[\mu F]$
System frequency	70	$[kHz]$
Simulation time step (T_s)	35.7	$[ns]$

The first test was step changes in the load power demands P_L. These changes were set as:

$$P_L = 0 \rightarrow 1100 \rightarrow 3300 \rightarrow -3300 \rightarrow 3300W \tag{A.1}$$

Each value of P_L was kept for 20 msec, and were created with $V_{LVS} = 660$ V. Figure A.1 shows the waveforms of the two currents I_1 and I_2, reference and actual voltage on the low voltage side of the HFT, and voltage commands ΔV_1 and ΔV_2 for this test.

It can be seen from Figure A.1 that the designed LQR controller could be tuned to operate DAB PECs with different voltage and power ratings. The results of this case showed that LQR controller was able to initiate accurate, fast and dynamic responses to step changes in the load power demands. Similar to the test results in Chapter 4, the actions of the designed LQR controller were able to create minor overshoots in the current I_1. Moreover, the actions of the designed LQR controller maintained negligible value of the current I_2 during and post each change in P_L.

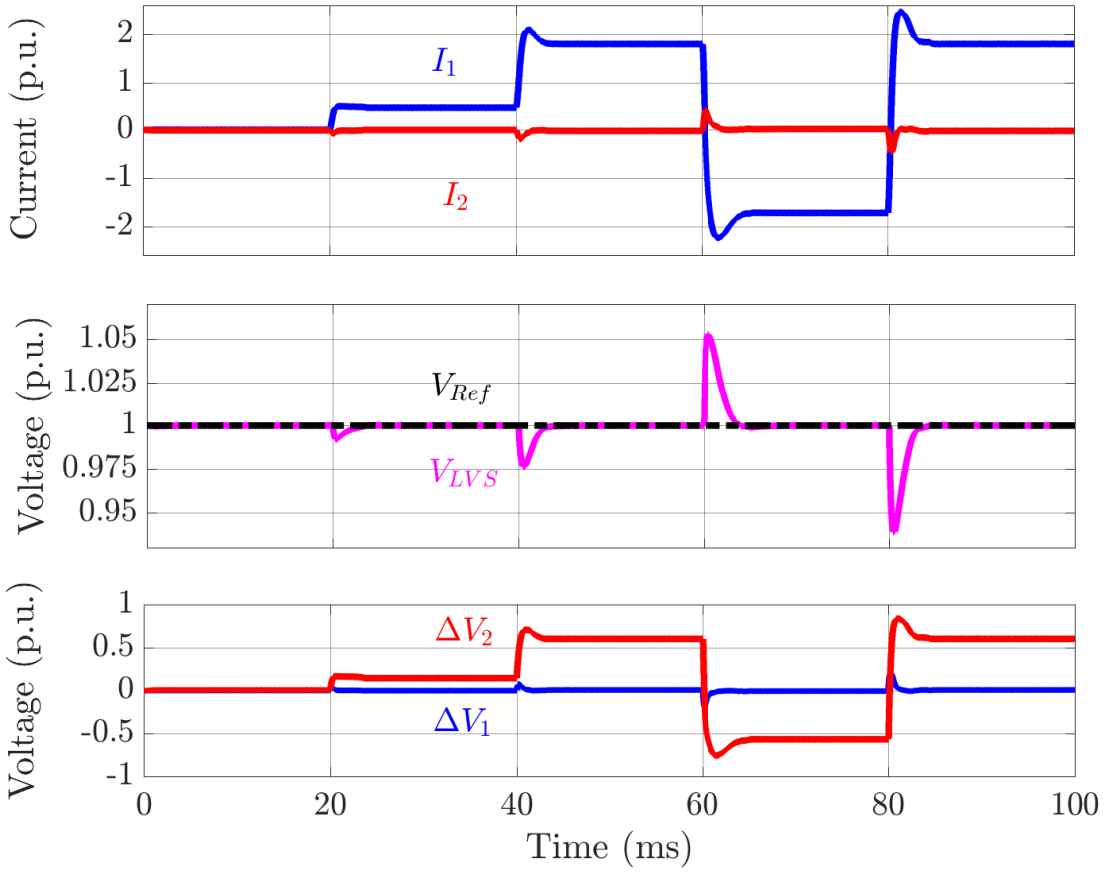

Figure A.1: Responses of the conventional DAB PEC with the designed LQR controller to step changes in load power demands. The per-unit currents I_1 and I_2 (base current is 5 A), per-unit reference and actual voltage on the low voltage side of the HFT (base voltage is 660 V), and per-unit voltage commands ΔV_1 and ΔV_2 (base voltage is 660 V).

Actions of the designed controller were also accurate in producing minor deviations in V_{LVS} from its reference value. Finally, actions of the LQR controller ensured small deviations in the voltages on both sides of the HFT, as indicated by $\Delta V1$ and $\Delta V2$. The results of this test demonstrated that the designed LQR was able to accurately operate DAB PECs with minor sensitivity to the voltage and power ratings, loading levels, and/or direction of the power flow.

The second test was conducted for step changes in the voltage V_{MVS} applied to the

medium voltage side of the HFT. The step changes in V_{MVS} were created each 20 msec. as:

$$V_{MVS} = 1 \rightarrow 0.9 \rightarrow 1 \rightarrow 1.1 \rightarrow 1\, p.u. \tag{A.2}$$

with the base voltage being 660 V. The step changes in V_{MVS} were created as P_L was kept at $P_L = 2.64$ kW. The waveforms of the two currents I_1 and I_2, reference and actual voltage on the low voltage side of the HFT, and voltage commands $\Delta V1$ and $\Delta V2$ for this test are shown in Figure A.2.

Figure A.2 shows that the actions of the LQR controller were able to adjust the current I_1 in response to the changes in V_{MVS} to maintain the power demands of the load. The changes in I_1 were fast, accurate, and with negligible overshoots. In addition, the designed LQR was able to to minimize the variations in I_2 and deviations in V_{LVS} from its command value. The small values of $\Delta V1$ and $\Delta V2$ confirmed that actions of the LQR controller reduced the deviations in the voltages on both sides of the HFT. The results of this test were in agreement with the results obtained from other tests, where the designed LQR controller was able to operate DAB PECs with minimum deviations in the voltages and currents on both sides of the HFT. The actions of the designed LQR controller were not impacted by the changes in V_{MVS}, loading level and/or direction of the power flow.

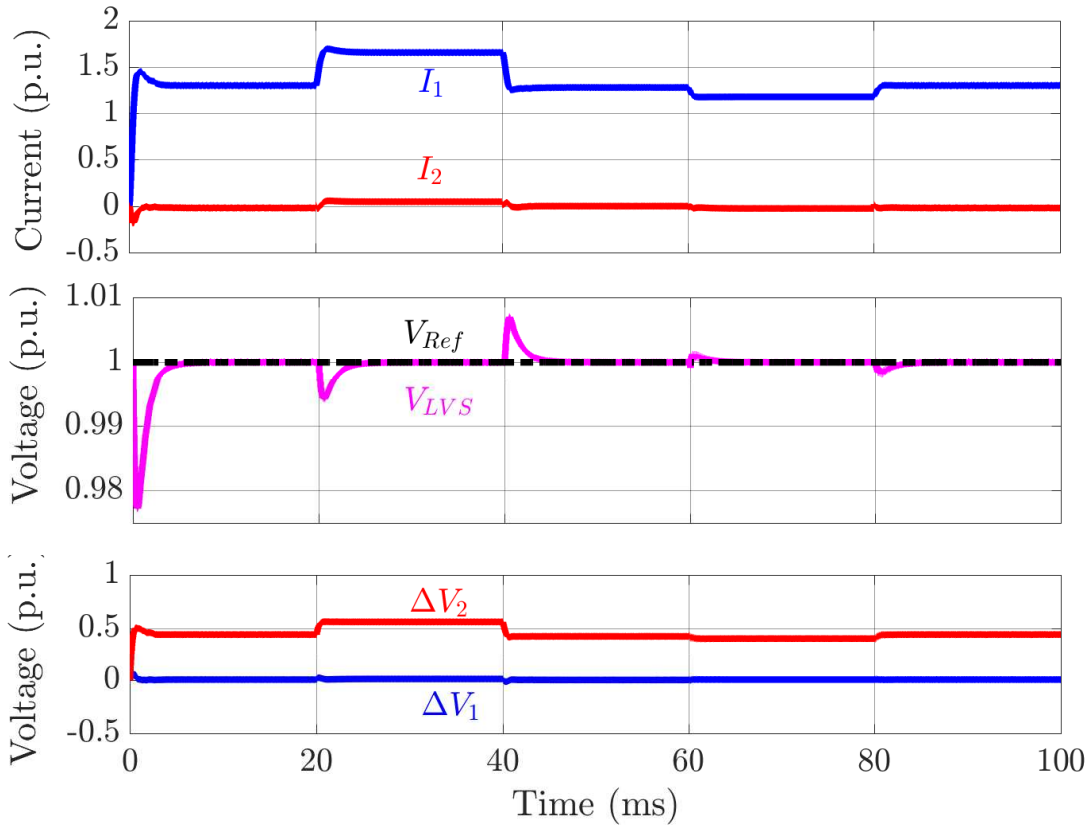

Figure A.2: Responses of the conventional DAB PEC with the designed LQR controller to step changes in the supply voltage while supporting a 2640 W load. The per-unit currents I_1 and I_2 (base current is 5 A), per-unit reference and actual voltage on the low voltage side of the HFT (base voltage is 660 V), and per-unit voltage commands ΔV_1 and ΔV_2 (base voltage is 660 V).

A.2 Combined DAB PECs

In some industrial applications, operating voltage and power ratings can be too large to be processed by a single DAB PEC. For these applications, multiple DAB PECs are usually used to reduce the voltage stresses and current carrying requirements of individual DAB PECs. Multiple DAB PECs can be connected in series, where the medium voltage side of each DAB PEC is connected in series to the next DAB PEC (voltage divider approach). The low voltage side of each DAB PEC is connected in

parallel with the low voltage sides of other DAB PECs (current divider approach).

This section presents test results for a system composed from 3 series-connected conventional DAB PECs. In these tests, V_{MVS} and P_L tripled in order to reflect the voltage and power ratings of this system. It should be noted that each DAB PEC is constructed using the parameters in Table 4.1. In this test, each DAB PEC has a LQR controller with a command voltage of one third of V_{MVS} , and a load demand of one third of P_L. The setting of each DAB PEC parameters have provided a matrix K (for each LQR controller) identical to that in equation (4.15).

The first test was step changes in the load fed by each DAB PEC. These changes in load demands were set as:

$$P_L = 0 \rightarrow 240 \rightarrow 750 \rightarrow -750 \rightarrow 750W \tag{A.3}$$

The changes in P_L were set to last for 20 msec. Figure A.3 shows the waveforms of the reference and actual voltage on the low voltage side of the HFT for each DAB PEC.

Figure A.3 shows that the LQR controllers were able to initiate accurate, fast and dynamic responses to step changes in the load power demands. The responses of LQR controller resulted in maintaining a close match between V_{REf} and V_{LVS} during and post each change in P_L. The results of this test demonstrated that the designed multiple LQR controllers could operate series-connected DAB PECs for higher voltage and power ratings. These results also demonstrated that the accuracy and response speed of the designed LQR controllers were impacted by the series connection of the DAB PECs and/or direction of the power flow.

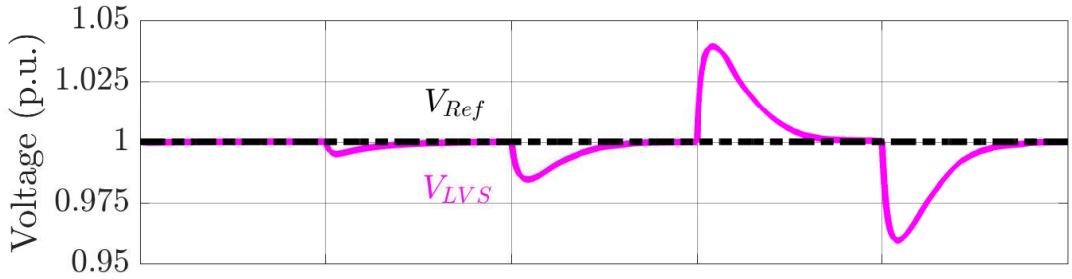

Figure A.3: Responses of three combined conventional DAB PECs with the designed LQR controller to step changes in load power demands. The per-unit reference and actual voltage on the low voltage side of the HFT (base voltage is 360 V).

The second test was conducted for step changes in the voltage (V_{MVS}) applied to the medium voltage side of the HFT in each of the three series-connected DAB PECs. The step changes in V_{MVS} were created each 20 msec. as:

$$V_{MVS} = 1 \rightarrow 0.9 \rightarrow 1 \rightarrow 1.1 \rightarrow 1\, p.u. \tag{A.4}$$

with the base voltage being 1080 V. The step changes in V_{MVS} were created as P_L was kept at $P_L = 0.6$ kW. The waveforms of the reference and actual voltage on the low voltage side of the HFT for this test are shown in Figure A.4.

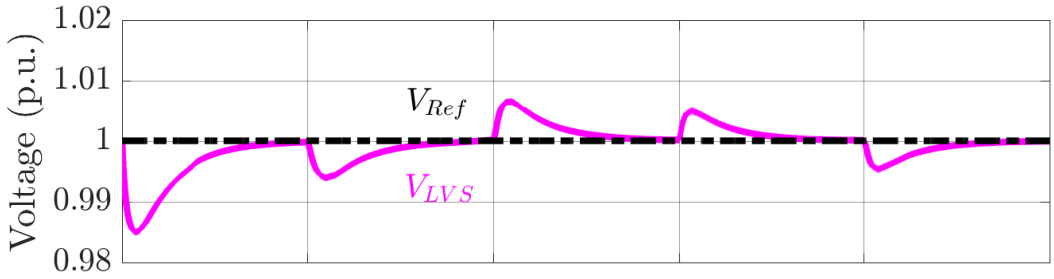

Figure A.4: Responses of three conventional DAB PECs with the designed LQR controller to step changes in the supply voltage while supporting a 600 W load. The per-unit reference and actual voltage on the low voltage side of the HFT (base voltage is 360 V)

It could be seen from Figure A.4 that the actions of the three LQR controllers were able to maintain the power demands of the load. The responses to the changes in V_{MVS} were fast, accurate, and with negligible overshoots. In addition, the designed LQR controllers were able to minimize the deviations in V_{LVS} from its command value. The results of this test were in agreement with the results obtained from other tests, where the designed LQR controllers were able to operate the series-connected DAB PECs with minimum deviations in the voltages and currents on both sides of the HFT. The actions of the LQR controllers were not impacted by the changes in V_{MVS} and/or loading levels.

Curriculum Vitae

Candidate:	Christian Gilles Richard
University attended:	Bachelor of Science in Engineering
	University of New Brunswick, Sept. 2013 - Apr. 2017
	Major: Electrical Engineering

Journal Publications:

[1] X. F. St-Onge, C. Richard, K. M. McDonald, S. A. Saleh, "Performance Testing of an Active Multiport DC Link for Grid-Connected PMG-Based WECSs," in *IEEE Transactions on Industry Applications*, vol. 54, no. 6, pp. 5579–5589, Nov./Dec. 2018

[2] S. A. Saleh, C. Richard, X. F. St-Onge, J. Meng, E. Castillo-Guerra, "Comparing the Performance of Protection Coordination and Digital Modular Protection for Grid-Connected Battery Storage Systems", in *IEEE Transactions on Industry Applications*, vol. 55, no. 3, pp. 2440–2454, May/June 2019

[3] C. Richard, K. McDonald, X. F. St-Onge, Saleh Saleh, "A New Isolated DCDC Converter for Discontinuous Input and Continuous Output", in *IEEE Transactions on Industry Applications*, vol. 55, no. 4, pp. 4215–4224, July/Aug. 2019

[4] S. A. M. Saleh, C. Richard, X. F. St-Onge, K. M. McDonald, E. Ozkop, L. Chang, B. Alsayid, "Solid-State Transformers for Distribution SystemsPart I: Technology and Construction", in *IEEE Transactions on Industry Applications*, vol. 55, no. 5, pp. 4524–4535, Sept./Oct. 2019

[5] S. A. Saleh, E. Ozkop, B. Alsayid, C. Richard, X. F. St. Onge, K. McDonald, L. Chang, "Solid-State Transformers for Distribution Systems–Part II: Deployment Challenges", in *IEEE Transactions on Industry Applications*, vol. 55, no. 6, pp. 5708–5716, Nov./Dec. 2019

[6] S. A. Saleh, X. F. St. Onge, C. Richard, E. Ozkop, S. Panetta, "Design and Testing of a Frequency-Selective Grounding for 3 Power Transformers", in *IEEE Transactions on Industry Applications*, vol. 56, no. 1, pp. 74–87, Jan/Feb 2020

Conference Publications:

[1] X. F. St. Onge, K. M. McDonald, C. Richard, S. A. Saleh, "A new multi-port active DC-link for PMG-based WECSs", in *Proceedings of the 2018 IEEE/IAS 54th I&CPS Technical Conference*, Niagara Falls, ON, May 2018

[2] S. A. Saleh, X. F. St. Onge, C. Richard, E. Ozkop, K. M. McDonald, S. Panetta, "Impacts of grounding and winding configurations on voltage harmonics in 3 power transformers", in *Proceedings of the 2018 IEEE/IAS 54th I&CPS Technical Conference*, Niagara Falls, ON, May 2018

[3] C. Richard, K. M. McDonald, X. F. St. Onge, S. A. Saleh, "Performance Evaluation of an Isolated DC-DC Converter with Discontinuous Supply", in *Proceedings of the 2018 IEEE/IAS Annual Meeting*, Portland, OR, Sept. 2018

[4] S. A. Saleh, C. Richard, X. F. St-Onge, J. Meng, E. Castillo-Guerra, "On the Comparison Between the Protection Coordination and Digital Modular Protection for Grid-Connected Battery Storage Systems", in *Proceedings of the 2018 IEEE/IAS Annual Meeting*, Portland, OR, Sept. 2018

[5] S. A. Saleh, E. Ozkop, B. Alsayid, C. Richard, X. F. St. Onge, K. McDonald, L. Chang, "Solid-State Transformers for Distribution Systems: Technology, Performance, and Challenges", in *Proceedings of the 2019 IEEE/IAS 55th I&CPS Technical Conference*, Calgary, AB, May 2019

[6] S. A. Saleh, X. F. St. Onge, C. Richard, E. Ozkop, S. Panetta, "Frequency-Selective Grounding for 3 Power Transformers", in *Proceedings of the 2019 IEEE/IAS 55th I&CPS Technical Conference*, Calgary, AB, May 2019

[7] S. A. Saleh, X. F. St. Onge, C. Richard, E. Ozkop, "dq0 PHT-Based Digital Differential Protection for 3 Converter Transformers", in *Proceedings of the 2019 IEEE/IAS Annual Meeting*, Baltimore, MD, Sept./Oct. 2019